REPORT DOCUMENTATION PAGE

Form Approved
OMB No. 074-0188

1. AGENCY USE ONLY (Leave blank)	2. REPORT DATE	3. REPORT TYPE AND DATE COVERED
	27-Feb-10	Final Report 01-May-2009 – 31-Jan-2010

4. TITLE AND SUBTITLE
Development of Multidisciplinary, Multifidelity Analysis, Integration and Optimization of Aerospace Vehicles

5. FUNDING NUMBERS
AFRL Contract FA9550-09-C-0135

6. AUTHOR(S)
Reisenthel, Patrick H., Allen, Theodore T., Lesieutre, Daniel J., and Lee, Soo Ho

7. PERFORMING ORGANIZATION NAME(S) AND ADDRESS(ES)
NIELSEN ENGINEERING & RESEARCH, INC.
2700 Augustine Drive, Suite 200
Santa Clara, CA 95054-2927

8. PERFORMING ORGANIZATION REPORT NUMBER
NEAR TR 657

9. SPONSORING/MONITORING AGENCY NAME(S) AND ADDRESS(ES)
Air Force Research Laboratory/AFOSR
875 N. Randolph St., Room 3112
Arlington, VA 22203

10. SPONSORING/MONITORING AGENCY REPORT NUMBER

11. SUPPLEMENTARY NOTES

12a. DISTRIBUTION/AVAILABILITY STATEMENT
Approved for public release; distribution unlimited.

12b. DISTRIBUTION CODE

13. ABSTRACT (*Maximum 200 Words*)

Report developed under STTR contract for topic AF08-BT03. The purpose of this work is to develop methods for representing, managing, and fusing information of various levels of fidelity within an engineering discipline and across multiple disciplines for a wide-range of analysis and design tools. An efficient, radial basis function-based extension of multifidelity sequential Kriging optimization was developed. This method, referred to as multifidelity sequential radial basis optimization (MFSRBO) addresses multicriteria optimization involving more than a single type of model representing more than a single discipline, and takes into account both the location in design space and the fidelity of further data acquisition/infill. Several variants of the method are discussed, and their potential assessed for future development. The application of MFSRBO is illustrated on a UAV wing design function integrating information from structural and fluid models. In the context of virtually any major computational (CAD/FEM) optimization, the proposed methods offer substantially reduced computational cost to arrive at the optimum solution. As a result, engineers and researchers can potentially solve more design problems in less time and achieve higher quality results at reduced costs.

14. SUBJECT TERMS	15. NUMBER OF PAGES
STTR Report, Global Optimization, Multiple Fidelity, Multidisciplinary Optimization, Metamodeling, Surrogate Systems, Uncertainty Management	45
	16. PRICE CODE

17. SECURITY CLASSIFICATION OF REPORT	18. SECURITY CLASSIFICATION OF THIS PAGE	19. SECURITY CLASSIFICATION OF ABSTRACT	20. LIMITATION OF ABSTRACT
UNCLASSIFIED	UNCLASSIFIED	UNCLASSIFIED	

DEVELOPMENT OF MULTIDISCIPLINARY, MULTIFIDELITY ANALYSIS, INTEGRATION, AND OPTIMIZATION OF AEROSPACE VEHICLES

Patrick H. Reisenthel,[¶] Theodore T. Allen,[§] Daniel J. Lesieutre[¶] and Soo Ho Lee[§]

[¶] Nielsen Engineering & Research, Inc.
2700 Augustine Drive, Suite 200
Santa Clara, CA 95054

[§] The Ohio State University
1971 Neil Avenue – 210 Baker Systems
Columbus, OH 43210

NEAR TR 657

27 February 2010

TABLE OF CONTENTS

FOREWORD

The present final report for AFOSR contract number FA9550-09-C-0135 describes the results of an STTR Phase I collaboration between Nielsen Engineering and Research (NEAR), Inc. and the Ohio State University (OSU). Dr. Patrick Reisenthel (NEAR) was the Principal Investigator for this effort. The OSU team was led by Prof. Theodore Allen. The present report includes contributions by Mr. Daniel Lesieutre (NEAR) and Mr. Soo Ho Lee (OSU), and is a comprehensive stand-alone report of the activities conducted as part of this STTR on the development of novel multifidelity modeling and optimization approaches applicable to multidisciplinary design and analysis of aerospace vehicles.

In this report, references to "the Team" or "our Team" pertain to the joint NEAR-OSU partnership. In addition to this report, and pending further results to be developed as part of Soo Ho Lee's Ph.D. dissertation, our Team intends to submit at least two papers for publication. The first of these papers, targeted for the *Journal of Global Optimization*, will focus on the single-fidelity version of radial basis sequential optimization. The second paper will be concerned with the multifidelity version and will be submitted to *Structural and Multidisciplinary Optimization*.[1]

1. SUMMARY

The development of revolutionary aerospace vehicles presents significant challenges. Cross-disciplinary integration offers potentially important advantages early in the design cycle, and to do so accurately and efficiently requires merging multiple levels of fidelity within an engineering discipline, as well as understanding the necessary degree of coupling between disciplines.

To address these demands our Team has developed methods and code for a radial basis function-based optimization alternative to multifidelity Kriging optimization. Like the Kriging-based method, our code involves more than a single type of simulation model. The approach can integrate data from multiple disciplines and takes into account both the location (in design space) and the fidelity of further data acquisition/infill.

Specifically, a study of radial basis functions in the context of multifidelity optimization is presented, including comparisons to prior modeling options and alternatives. We describe a general multifidelity framework and specific methods, including hybrid methods whose convergence is established. Numerical results on test problems are used to compare sequential radial basis optimization (SRBO) versus other methods. The results indicate that methods based on radial basis functions can compete with Kriging methods in relation to efficiency and repeated identification of global optimum solutions. As a result, our proposed SRBO might be preferred because of reduced computational overhead, improved numerical stability, and flexibility in terms of modeling uncertainty intervals. The example of an aeroelastic wing design using two levels of fidelity and two disciplines is used to demonstrate the feasibility of the proposed approach. The report concludes with a discussion of the results and opportunities for future research.

Overall, the proposed methods offer substantially reduced computational cost to arrive at the optimum solution. As a result, there is a potential for engineers and researchers to solve more design problems in less time and achieve higher quality results at reduced costs.

2. INTRODUCTION

The development of increasingly more complex and integrated aerospace vehicles that are capable of a variety of missions is leading engineers and scientists to consider nonconventional airframes, new structural and propulsion concepts and their interactions early in the design cycle. The technical

1 We also anticipate at least one paper presentation at an AIAA meeting on the aeroelastic wing design problem.

challenges faced in the design of these revolutionary air vehicles range from considerations of extreme environments (e.g., hypersonic/transatmospheric vehicles) to large dynamic shape variations of micro UAVs. This greater range of design options must be examined in cross-disciplinary terms, where individual disciplines are allowed to challenge the constraints of other disciplines. Cross-disciplinary design space exploration is needed to reduce uncertainty and increase knowledge in order to make better decisions. The large dimensionality of such a design space traditionally requires the use of low-fidelity methods at the conceptual design stage, but there is a need to incorporate high-fidelity analysis tools early in the design process. Mixed fidelity models are an enabling technology, allowing the design of individual system components to be understood within the broader context of a full system. Increased computational power and the proliferation of new unmanned aerial vehicle designs have been driving forces in the development of variable fidelity frameworks over the last decade. Yet, a number of fundamental issues in multifidelity computing remain unresolved.

Advanced aerospace vehicle design methods must fuse data from multiple sources and various levels of fidelity. In a multifidelity framework, the resolution and fidelity of simulations should be tailored to the requirements of the analysis. There are many factors to consider, including the spatial resolution, temporal resolution, physical processes being modeled, the number of objects, number of attributes of each object, and the degree of interaction between these objects (Gardner and Hennigan, 2003).

High-fidelity methods are typically more expensive, and must be used sparingly out of practical necessity. Other factors to consider are that high-fidelity analyses are assumed to be more accurate, but may not always be, and that there are often difficulties related to obtaining good gradients. For example, there might be integer/discrete variables associated with gross topological changes, e.g., number of compressor stages, number of engines, control surfaces and so on. These amount to major discontinuities ("cliff edges," in Jarrett's, 2006, terminology) which computationally efficient gradient-based design optimization methods cannot cross.

An obvious advantage of low-fidelity methods is that they are computationally inexpensive and fast. More rarely mentioned are the potential benefits of low-fidelity methods in a multifidelity framework, namely that they enable effective design exploration, not merely because of their speed, but as an aid to escape noisy local optima due to the nonsmooth nature of the design space, a common occurrence in the case in high-fidelity analyses. Low-fidelity methods enable safe transit between local optima, effectively tunneling back and forth through the cliff edges that discrete variable problems bring about (Jarrett, 2006). The disadvantages of low-fidelity tools are that they may produce inaccurate results. Also, low-fidelity tools may not work for unconventional designs or strongly nonlinear regimes (Wintzer et al., 2006), or may not be able to produce the quantities of interest (e.g., aerodynamic drag).

A significant issue in multidisciplinary frameworks is the difficulty in specifying consistency between models. A low-fidelity and high-fidelity model are said to be *weakly consistent* if "the projection of the state of the higher resolution model to the space of the lower resolution model is sufficiently close to the state of the low resolution model" (Gardner and Hennigan, 2003). In many applications, lower fidelity refers to lower resolution, but also different methodologies altogether involving significant approximations, not only missing detail but also missing physics (e.g., absence of chemical reactions, aeroelastic/unsteady effects, viscosity, or turbulence). In such cases, one cannot guarantee even *weak consistency.*

True integration of the results from codes of varying fidelity poses a number of challenges. One of them is the fact that prediction codes of varying fidelity levels use different input parameterizations and, therefore, operate in different spaces (Robinson et al. 2006a,b). Another challenge is the development of effective strategies when low- and high-fidelity models are not consistent, or when weak consistency is satisfied only in a small region of the design space, therefore limiting the efficiency of current multifidelity frameworks and, potentially, the breadth of design options being considered. The question of optimal sampling of the design space given limited resources is a critical one that is fundamentally linked to the characterization of uncertainty and uncertainty requirements. Specifically, there is a need to

develop rigorous approaches addressing not only where to sample the design space, but also at what level of fidelity.

In the past decade, there have been numerous implementations of variable fidelity ideas based on the concept of "bridge functions" as a re-anchoring framework to correct low-fidelity analyses to approximate the results of high-fidelity analyses. The "beta" factor initially proposed by Chang et al. (1993) is introduced as a local multiplicative factor, although many researchers (e.g., Hatanaka et al., 2006, Ghoreyshi et al., 2008) have found it advantageous to implement the additive form of the correction. These schemes incorporate Taylor expansion-based corrections between the low- and high-fidelity models, requiring the design space to be smooth, and require updates where both low- and high-fidelity data must be available at the same point. These factors tend to result in relatively frequent high-fidelity updates and, therefore, only modest improvements in computational savings over conventional optimization. While useful for establishing provable convergence to high-fidelity results/optimization, the local correction method has a tendency to limit the step sizes taken in optimization and, more generally, curtails the size of the design space exploration.

As pointed out in Forrester et al. (2009), efficient global optimization revolves around being able to successfully balance exploration and exploitation. Thus, there is a need for a multifidelity framework allowing bold optimization steps. The present work considers both hierarchical[2] and integrated[3] variable-fidelity metamodeling methods whose uncertainty is reduced with each evaluation. In this work, a radial basis function embodiment of these ideas is used to benchmark performance versus other methods and to demonstrate efficient multifidelity multidisciplinary optimization.

3. OBJECTIVES

Aerospace finite element method (FEM) and computational fluid dynamics (CFD) simulations continue to increase in fidelity/realism. Yet, even as computer speeds increase, the most realistic models (e.g., of turbulent flows) are still relatively slow computationally, making thorough optimization difficult. In fact, the gap between the computational speed of low-fidelity models and high-fidelity models continues to increase also. As a result, methods for multifidelity optimization which leverage efficient low-fidelity models promise to enable thorough optimization.

In the years following Jones, Schonlau, and Welch (1998), there has been growing interest in optimization using global metamodels, e.g., Kriging or radial basis functions. Unlike other design of experiments (DOE) methods like sequential response surface methods, global metamodels can integrate and generate predictions over the entire design space. As a result, they can integrate an entire data set from an entire design optimization process which can involve human participation in the process. Nonglobal metamodeling approaches for multifidelity optimization are described in Singh and Grandhi (2010). Advances in global metamodeling using radial basis functions include Gutmann (2001), Holmström (2008), Floudas and Gounaris (2009), and Antanas (2010). Our Team's selection of the radial basis function approach is based on its suitability for use in efficient global optimization and its extension to the multifidelity context (see Section 4).

The broad objective of this work is to pioneer innovative methods for representing, managing, and fusing information of various levels of fidelity within an engineering discipline and across multiple disciplines for a wide-range of analysis and design tools. The specific objectives of this study include **(1)** developing a multifidelity multidisciplinary framework through alternative formulations to previous methods, computational results, and rigorous mathematical results, **(2)** extending Huang et al.'s (2006) multifidelity design space sampling strategy to manage system updates within integrated and hierarchical global metamodeling approaches, **(3)** extending the rigorous convergence results from Schonlau (1997) to multifidelity optimization in the context of radial basis function methods and Kriging models,

2 also referred to in this work as "cascading model"
3 referred to in this work as the "augmented dimensionality model"

(4) developing adaptive methods to achieve probabilistic convergence results and enhance performance. The purpose of this STTR Phase I is to demonstrate the feasibility of the proposed approach through its application to a baseline problem involving at least two interactive disciplines and two levels of fidelity. Therefore, objective **(5)** is the application of the proposed methods to a flying wing-type UAV design function integrating information from structural and fluid models.

4. METHODS

This section describes in detail the methods, assumptions, and procedures used in this work. We begin (Section 4.1) with an overview of the optimization process, contrasting the traditional approach and the multifidelity framework envisioned in this work. This is followed (Section 4.2) by a discussion of surrogate models, including the rationale for our choice of radial basis functions. Section 4.3 describes the optimization methods, and Section 4.4 documents the computational analyses used in this work.

4.1 OVERVIEW

In the conventional view of the design process, decisions evolve over time. At the conceptual design stage and, increasingly, in preliminary design, a large array of options and cross-disciplinary trades are considered, even though the knowledge of the system is necessarily imprecise (Lewis and Mistree, 1998). This is traditionally the *design space exploration* phase, where individual disciplines must be able to challenge the constraints of other disciplines (Holden and Keane, 2004) in order to come up with effective solutions. An outcome of these analyses is, traditionally, to narrow down the design space to smaller, more manageable portions which are subsequently investigated in more detail. The intermediate level of fidelity, though more expensive, is then used to refine the analysis, add geometric detail, and increase the physical fidelity of the models used, thus reducing the uncertainty in the design. Cross-disciplinary interactions are retained in the MDO methods used, but a smaller portion of the design space is considered, to make this tractable in spite of the higher costs. Finally, the detailed design stage is used to further refine the analysis, narrowing the design to a handful of options.

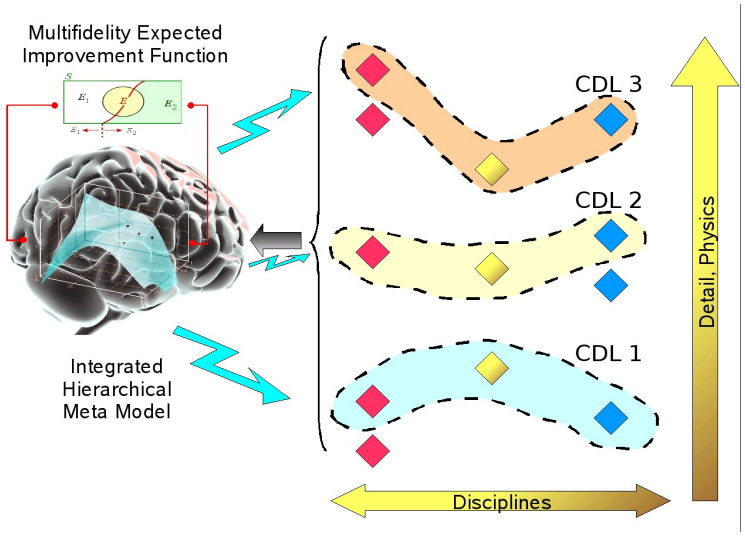

Figure 1. Integrated Hierarchical Framework.

In contrast to the conventional view, the proposed multifidelity multidisciplinary framework (illustrated in **Figure 1**) is a true integrated hierarchical model which takes into account (merges) the information from multiple fidelity levels and manages this information in order to achieve optimal sampling of the design space, both in terms of design variables and level of fidelity. The right-hand side in **Figure 1** represents analysis codes spanning three hypothetical disciplines, e.g., fluids, structures, and guidance and

control. Each analysis code is represented by a ◇ symbol and is ranked according to its level of fidelity, i.e., the level of the physics included in the model and the level of geometric detail. Within the multidisciplinary multifidelity framework, codes with compatible fidelity levels are first coupled together using cross-disciplinary links (CDL). Such groupings are the staple of multidisciplinary optimization (MDO) and include not only the code associations but also the nature of the coupling between them. Within each group, not only are variables appropriately exchanged between disciplines, but the processes for information exchange/update are well-defined. For example, the disciplines within a group can be tightly integrated or loosely coupled, physical interactions accounted for explicitly or through subiterations between codes, and so on. The left-hand side of the figure symbolizes the two key elements which underlie the proposed approach. The first is the merging of all multifidelity data into a global probabilistic response surface-based metamodel (see Section 4.2.2). This "Integrated Hierarchical Metamodel" builds on the foundation provided by multifidelity radial basis function (RBF) data fusion methods (Reisenthel et al., 2006*a*), and optimization methods using probabilistic RBF networks (see, e.g., Reisenthel and Lesieutre, 2007). The second element and a key addition to these ideas is the use of a Multifidelity Sequential Kriging Optimization (MFSKO)-like "Expected Improvement Function" (Section 4.3.4) to manage when high-, medium-, and low-fidelity analysis tools are appropriate as the "next move" in design space exploration/exploitation and metamodel updates. The goal of balancing exploration and exploitation in a mathematically rigorous way is achieved by using an integrated criterion which determines both the location and fidelity level of subsequent searches. This criterion is based on Kennedy and O'Hagan's (2000) original work, and subsequent refinements by OSU members of our Team (Huang et al., 2006, Schenk et al., 2005).

The work presented in this report focuses primarily on the multifidelity aspects of aerospace vehicle analysis and design. Thus, the "isofidelity"-groupings depicted in **Figure 1** represent an encapsulation of existing analysis tools, solution methods, and information exchange processes which can operate independently of each other. The central question addressed in this work is how to merge and manage the information from these multiple fidelity groupings.

4.2 SURROGATE MODELS

At the heart of the multifidelity multidisciplinary framework depicted in **Figure 1** reside (1) a dynamic metamodel and (2) an intelligent management tool. As shown in Section 4.2.1, the choice of surrogate for the metamodel has a number of consequences which must be taken into account. Section 4.2.2 details the multifidelity radial basis function surrogate models used in this work.

4.2.1 BACKGROUND/RATIONALE

A summary comparing the pros and cons of four different classes of surrogate-based methods is provided in **Table 1**. This summary organizes information gleaned in large part from the review papers of Forrester et al. (2009) and, to a lesser extent, Queipo et al. (2005), and supplemented with our own experience. The table is organized as follows. The four classes of methods (polynomial, radial basis, Kriging, and support vector regression) are listed across the top, with their attributes listed by row. These key attributes are categorized according to (a) the forming of the metamodel surrogate, (b) considerations pertinent to optimization, and (c) multifidelity modeling. While many of the table entries are qualitative (e.g., "Low" vs. "Med. Low"), their intent is to give a sense of the relative performance of one method over another. Whenever possible, this sense of performance is quantified in terms of scaling with respect to number of points, search space dimensionality, and so on. Particular method variants may cross boundaries, and not all methods are represented, so this is not intended to be a comprehensive guide but, rather, a reference to help explain where the proposed methods (highlighted) fit within the spectrum of existing approaches.

Table 1. Characteristics of various surrogate-based methods & assessment of suitability for multifidelity multidisciplinary optimization.

		PRG	MLS	RBF	qParam. RBF	Param. RBF	KRG	Blind KRG	SVR	Param. SVR
Metamodel Construction	Assumption requirements	High	Medium	Med. Low	Low	Low	V. Low	V. Low	Med. Low	V. Low
	Landscape complexity	Low	Medium	Med. High	High	High	V. High	V. High	Med. High	V. High
	Ability to incorporate derivatives	Yes	Yes	Yes	Yes	Yes	Yes	Yes	Unknown	Unknown
	Generalization error	Medium	Low	Med. Low	Low	Low	V. Low	V. Low	Low	V. Low
	Time spent training or retraining the metamodel	Low	High	Low	Low	Medium	High	V. High	V. High	V. High
	Solution effort in terms of number of parameters searched (independently of GCV)*	0	0	0	0	1	$2k$	$2k^2 + 1$	$2n$	$2n + 1$
	Number of potential regressors, given m data points†	$\frac{(m+d)!}{m!\,d!}$	$\frac{(m+d)!}{m!\,d!}$	m	m	m	m	m	m	m
	Maximum number of data points m	High	V. High	< 1000	< 1000	< 1000	< 500	< 500	High	High
	Estimate# of maximum design space dimensionality k	$k < 20$	$k < 20$	High	High	High	$k < 20$	$k < 20$	High	High
	Ease of implementation	V. High	High	High	High	Medium	Medium	Low	Low	Low
	Possibility of error prediction estimates	Yes	Yes	Yes	Yes	Yes	Yes	Yes	Yes	Yes
	Current availability of error estimates	Unknown	Unknown	Yes	Yes	Unknown	Yes	Yes	Yes	Yes
Optimization	Adaptivity (ability to fit complex local behavior)	Low	Medium	Medium	High	High	High	High	Low	High
	Cost of search	Low	High	Low	Low	Low	Low	Low	Low	Low
	Basic effort associated with a 2-stage infill, in terms of number of parameters searched (independently of GCV)*	0	0	0	0	1	$2k$	$2k^2 + 1$	$2n$	$2n + 1$
	1-stage¶ infill effort in terms of number of parameters searched (independently of GCV)*	Unknown	Unknown	$k + 1$	$k + 1$	$k + 2$	$3k + 1$	$2k^2 + k + 1$	$2n + k + 1$	$2n + k + 2$
	Overall suitability for optimization	Med. Low	Low	Medium	High	High	Med. High	Medium	Low	Low
	Suitability for global optimization	V. Low	Low	Medium	High	High	Med. High	Medium	Unknown	Unknown
Multifidelity	Approximation model or surrogate management framework used	Affine correction process Trust region methods •*low level of complexity between fidelity levels* •*lack of flexibility in terms of point/fidelity selection*		•Kennedy - O'Hagan •Dimensionality augmentation + Least Squares Estimation •*models complex relationships* •*flexible point/fidelity selection* •*fast*			Co-Kriging (Kennedy-O'Hagan + Kriging) •*potentially high level of complexity between fidelity levels* •*flexible point/fidelity selection*		Unknown	

Notes: * assumes k-dimensional design space and n support vectors
† assumes m data points and polynomial of degree d
¶ (conditional lower bound approach); estimated scaling (except KRG, from Forrester et al., 2009).
# Maximum dimensionality for PRG and MLS limited due to large number of regressors; maximum dimensionality for KRG and Blind KRG limited due to computational effort; potential maximum dimensionality for RBF variants is uncertain, although our Team has successfully tested interpolating RBF solutions of random data in 100+ dimensions.

It is important to keep in mind that the applicability or optimality of a given method is problem-dependent. Thus, for example, a method which seems unattractive due to computational demands (e.g., if it involves layer of optimization upon layer of optimization) may be worth the effort, depending on how costly a single high-fidelity evaluation is. Paradoxically, Forrester et al. (2009) note that, for those very applications, i.e., those most likely to be solved in a highly parallel computing environment, "setting up and searching a surrogate of any kind can (become the) bottleneck. (...) This fact will always limit the amount of time we can dedicate to the building and searching of surrogates."

In part for this reason, the multifidelity multidisciplinary optimization approach recommended by our Team centers on radial basis function (RBF) surrogation, including several of its variants (fixed basis RBF, quasi-parametric RBF, and parametric RBF). As depicted in **Table 1**, this class of methods appears to offer qualities which very nearly approach those of Kriging (in terms of modeling ability, flexibility, and generalization properties) but with significant advantages in terms of performance. The RBF class of surrogates covers a wide range of methods, from simple fixed basis RBF to fully parametric RBF approaching the complexity of Kriging. Within this class, we have the freedom to trade generality for performance, depending on which parameters are solved by optimization (parametric RBF) versus which parameters are fixed (RBF). It is argued that a particularly efficient middle ground is the quasi-parametric RBF framework, where metaparameters evolve according to a prescribed algorithm. Such algorithms may be rooted in heuristics and are designed to ensure adaptivity while maintaining high performance.

4.2.2 MULTIFIDELITY RADIAL BASIS FUNCTION SURROGATE MODELS

In this section, multifidelity modeling issues are described for models involving radial basis functions. We describe two modeling formulations and variance and bias errors. The first derives from previous research in which radial basis functions model the systematic errors of each surrogate system in relation to higher fidelity systems. The second formulation treats fidelity as a design dimension and adjusts the specific scaling in the radial function.

4.2.2.1 Modified Kennedy and O'Hagan Scheme

The first and primary modeling formulation is adapted from Kennedy and O'Hagan (2000) involving both linear and Kriging models. This was the approach used in Huang, Allen, Notz, and Miller (2006). The "cascading" formulation is:

$$f_l(\mathbf{x}) = f_{l-1}(\mathbf{x}) + \delta_l(\mathbf{x}) \qquad (l = 2, 3, \ldots, m) \qquad \textbf{(1)}$$

where f_l is the function evaluated at fidelity level l and $\delta_l(\mathbf{x})$ is independent of $f_1(\mathbf{x}), f_2(\mathbf{x}), \ldots, f_{l-1}(\mathbf{x})$ and $\mathbf{x}$ is a d dimensional decision vector. Hypothetically, different levels of l also could be different levels of a discrete factor for the same fidelity level. For convenience in the notations below, we also let:

$$f_1(\mathbf{x}) = \delta_1(\mathbf{x}). \qquad \textbf{(2)}$$

Note that for $l = 2, 3, \ldots, m$, $\delta_l(\mathbf{x})$ can be understood as the "systematic error" of a lower-fidelity system, $(l–1)$, as compared to the next higher-fidelity system, l. In these cases, $\delta_l(\mathbf{x})$ is usually small in scale as compared to $f_l(\mathbf{x})$, otherwise there will be no reason for the lower-fidelity system to exist. Of course, in some cases, physics may be missed in low-fidelity model(s) and $\delta_l(\mathbf{x})$ will be large.

In radial basis metamodeling, the response is assumed to be a linear model. We use another radial basis function to model the departure of the lowest-fidelity system, $\delta_1(\mathbf{x})$, as well as the difference between systems, $\delta_l(\mathbf{x})$ $(l = 2, 3, \ldots, m)$. Therefore, we have

$$\delta_l(\mathbf{x},S_1,\ldots,S_m) = \mathbf{b}(\mathbf{x},S_1,\ldots,S_l)^T\boldsymbol{\beta}_l + \varepsilon_l \quad (l = 1, 2, \ldots, m) \qquad \textbf{(3)}$$

where $\mathbf{b}_l$ and $\boldsymbol{\beta}_l$ are the basis functions and coefficients, respectively, of a linear model. Also, the sets $S_1,\ldots,S_m$ contain the input points for selected past runs at the m levels of fidelity. In general, not all previous runs are included in the model so that there can be lack of fit estimation.

The linear model portion is richer in Eq. (3) than in Huang, Allen, Notz, and Miller (2006) because it contains dependence on design points. The basis functions of the linear model here are radial centered on the design points. By basing the model centering on design points there is no nonlinearity associated with picking runs.

In our implementations, we use Gaussian basis functions or, alternatively, reciprocal multiquadrics centering in both cases on k selected runs. In this report, we focus somewhat arbitrarily on Gaussian basis functions but our experiences with the use of multiquadrics were similar. For a single fidelity level the Gaussian basis function is:

$$\phi(\mathbf{x},\mathbf{x}_j) = \exp[-\gamma(\mathbf{x}-\mathbf{x}_j)'(\mathbf{x}-\mathbf{x}_j)] \qquad (j = 1, 2, \ldots, k). \qquad \textbf{(4)}$$

where γ is an adjustable scale parameter. In this report, we focus on γ as a fixed parameter. Yet, the adjustment of γ as the algorithm evolves is considered promising for further improvements to numerical results on test problems. In general, our Team feels that desirable algorithms that increase γ as the algorithm are most likely to foster improved results.

Therefore, the general form of the prediction model at the point $\mathbf{x}$ at fidelity level l is:

$$f_l(\mathbf{x}) = \sum_{i=1,\ldots,l} \sum_{j \subset S_i} \phi(\mathbf{x}_i,\mathbf{x}_j)\beta_{i,j} \quad . \qquad \textbf{(5)}$$

With these assumptions, the linear model design matrix, $\mathbf{X}$, is somewhat sparse. For example, with three fidelity levels and k_1, k_2, and k_3 runs included in the model and n_1, n_2, and n_3 total runs at each of three fidelity levels, the $\mathbf{X}$ matrix is:

$$\begin{bmatrix}
\phi(\mathbf{x}_1,\mathbf{x}_1) & \cdots & \phi(\mathbf{x}_1,\mathbf{x}_{k_1}) & & & & & & \\
\vdots & \ddots & \vdots & & & \mathbf{0} & & & \mathbf{0} \\
\phi(\mathbf{x}_{n_1},\mathbf{x}_1) & \cdots & \phi(\mathbf{x}_{n_1},\mathbf{x}_{k_1}) & & & & & & \\
\phi(\mathbf{x}_{n_1+1},\mathbf{x}_1) & \cdots & \phi(\mathbf{x}_{n_1+1},\mathbf{x}_{k_1}) & \phi(\mathbf{x}_{n_1+1},\mathbf{x}_{k_1+1}) & \cdots & \phi(\mathbf{x}_{n_1+1},\mathbf{x}_{k_1+k_2}) & & & \\
\vdots & \ddots & \vdots & \vdots & \ddots & \vdots & & & \mathbf{0} \\
\phi(\mathbf{x}_{n_1+n_2},\mathbf{x}_1) & \cdots & \phi(\mathbf{x}_{n_1+n_2},\mathbf{x}_{k_1}) & \phi(\mathbf{x}_{n_1+n_2},\mathbf{x}_{k_1+1}) & \cdots & \phi(\mathbf{x}_{n_1+n_2},\mathbf{x}_{k_1+k_2}) & & & \\
\phi(\mathbf{x}_{n_1+n_2+1},\mathbf{x}_1) & \cdots & \phi(\mathbf{x}_{n_1+n_2+1},\mathbf{x}_{k_1}) & \phi(\mathbf{x}_{n_1+n_2+1},\mathbf{x}_{k_1+1}) & \cdots & \phi(\mathbf{x}_{n_1+n_2+1},\mathbf{x}_{k_1+k_2}) & \cdots & \cdots & \cdots \\
\vdots & \ddots & \vdots & \vdots & \ddots & \vdots & \vdots & \ddots & \vdots \\
\phi(\mathbf{x}_{n_1+n_2+n_3},\mathbf{x}_1) & \cdots & \phi(\mathbf{x}_{n_1+n_2+n_3},\mathbf{x}_{k_1}) & \phi(\mathbf{x}_{n_1+n_2+n_3},\mathbf{x}_{k_1+1}) & \cdots & \phi(\mathbf{x}_{n_1+n_2+n_3},\mathbf{x}_{k_1+k_2}) & \cdots & \cdots & \cdots
\end{bmatrix}$$

In our numerical results, we fitted Eq. (5) by solving the normal equations using singular value decomposition (SVD) and ANSI C code. This code was significantly modified from code in Press, Teukolsky, Vetterling, and Flannery (2007). The modifications include facilitating multivariate modeling, covariance estimation, and error prediction.

The modified version is order $(n_1 + \ldots + n_m)^3$ but it requires generally negligible computing time compared with likelihood optimization in sequential Kriging optimization (Huang, Allen, Notz, and Miller 2006). Also, linear model estimation using SVD is generally more reliable and reproducible in part because of limited sensitivity to numerical issues.

4.2.2.2 An Alternative Augmented Dimensionality Formulation

Our team also considered alternative modeling formulations for addressing fidelity based on scaling inputs (Reisenthel et al., 2006). In some of these formulations, global adjustments to distances are made based on the differences between fidelity levels of the runs. Assume that $\mathbf{f}(i)$ is a $1 \times m$ vector with a 1 when i is the fidelity level of run i or 0 otherwise. In this approach, we consider adjustable parameters, $\gamma_i \geq 0$, for each of the design dimensions $i = 1,\ldots,d$ and $G_{ij} \geq 0$ for all fidelity levels $j = 1,\ldots m$ and $i = 1,\ldots m$. The revised density is:

$$\phi(\mathbf{x}_i,\mathbf{f}(i),\mathbf{x}_j,\mathbf{f}(j)) = \exp\{-\textstyle\sum_{k=1}^{d} \gamma_i \left(x_{k,i} - x_{k,j}\right)^2 - G_{ij}\|\mathbf{f}(i) - \mathbf{f}(j)\|^2\} \qquad \textbf{(6)}$$

where $\mathbf{x}_{k,i}$ is the k^{th} element of the vector $\mathbf{x}_i$. The model is simply:

$$f(\mathbf{x},q) = \sum_{j=1,\ldots,n} \phi[\mathbf{x},q,\mathbf{x}_j,\mathbf{f}(j)]\beta_j \qquad \textbf{(7)}$$

And the design matrix is:

$$\mathbf{X} = \begin{bmatrix} \phi(\mathbf{x}_1,r_1,\mathbf{x}_1,r_1) & \cdots & \phi(\mathbf{x}_1,r_1,\mathbf{x}_n,r_n) \\ \vdots & \ddots & \vdots \\ \phi(\mathbf{x}_n,r_n,\mathbf{x}_1,r_1) & \cdots & \phi(\mathbf{x}_n,r_n,\mathbf{x}_n,r_n) \end{bmatrix}$$

where we have assumed that all runs have been included in the model as an example. Therefore, Eq. (6) would represent a saturated model that generally passes through all of the design points.

This alternative, more concise formulation has the disadvantage that the G_{ij} weight parameters must be adjusted heuristically. Also, there is no guarantee that the process will converge to accurate models of the bias or systematic errors or the predictions of the highest fidelity model will converge. Yet, the augmented dimensionality approach includes far fewer parameters to be estimated and can be expected to offer efficiency advantages for cases in which assumption parameters match problem properties closely.

4.2.2.3 Modeling Prediction Variance

A possible advantage of Kriging models over radial basis functions is that they provide a model of mean and uncertainty even if the model passes through all the design points. Kennedy and O'Hagan (2000) and others have clarified the Bayesian nature of the intervals. Yet, the interpretation and validity of the derived intervals in realistic cases is not fully understood. At the same time, the computational performance in test problems of methods based on these Kriging error estimates appears to be good.

By contrast, the radial basis functions considered in previous sections are associated with regression type intervals. If the prediction model passes through all the design points, the standard regression intervals indicate zero prediction errors at all points. This follows because the standard intervals are based on so-called variance errors and therefore derive entirely from the assumed repeatability or random errors. We consider four possible approaches to address predictions of prediction uncertainty:

1. Assumed random errors – Some of the computational results from the team derived from ad hoc assumptions of random error standard deviation, σ, inserted into the prediction variance formula:

   $$\hat{\sigma}_l^2(x) = \text{Var}[y_{prediction}(\mathbf{x},l)] = \sigma_0^2\mathbf{b}(\mathbf{x},S_1,\ldots,S_l)^{\text{T}}(\mathbf{X}'\mathbf{X})^{-1}\mathbf{b}(\mathbf{x},S_1,\ldots,S_l). \qquad \textbf{(8)}$$

   This approach has some intellectual coherence in the context of FEM. This follows because there is often a known or typical uncertainty associated with computer code, e.g., related to the mesh size. Yet, the errors are not like typical repeatability errors.

2. Simply estimated random errors – A selected set of runs can be dropped from the model and used for estimating σ as is common in regression. In our computational results, we simply drop the most recently collected r runs from fitting. The standard Analysis of Variance estimate of the random error is then:

   $$\hat{\sigma}_0 = \sqrt{[(\boldsymbol{Y} - \boldsymbol{X}\boldsymbol{\beta})^T][(\boldsymbol{Y} - \boldsymbol{X}\boldsymbol{\beta})]/(n-r)} \qquad \textbf{(9)}$$

   which is based on an equal variance assumption as is standard in regression.

3. PRESS estimated random errors – The standard regression cross validation method of leaving out each observation, fitting with the others, and then rotating can be applied to estimate σ. This estimate is based on an average of calculations from Eq. (9).

4. Bias plus variance – Research by the OSU members of our Team has recently invented formulas for the variance and the bias. Such approaches are well-founded and make reference to high-order polynomial true models. They offer an intellectually coherent way to assign uncertainty even for cases like FEM with known perfect repeatability. Tseng (2007) provides several useful formulas.

Option 4 is the most attractive. However, in practice estimating bias errors requires the assumption of the model form of the true model, e.g., a fourth-order polynomial, and a distribution of the unknown coefficients. The associated arbitrariness of related assumptions makes these methods seem less attractive. Yet, Kriging models have associated ambiguities also relating to the validity and convergence of the assumed correlation parameters. At present, we focus on options (1) and (2) from the above list and leave options (3) and (4) for future research.

4.3 OPTIMIZATION METHODS

This section describes the central optimization problem and solution method framework. The framework is based on sequential optimization using radial basis function metamodels. It is based on a search after every computational analysis[4] for the location of the next run in the parameter and fidelity space that maximizes the expected improvement in a manner similar to Huang, Allen, Notz, and Miller (2006). Next, the expected improvement function is described and method variations based on it are defined. Finally, the developed Visual Basic, ANSI C, and Octave codes developed in this work are briefly characterized.

4.3.1 THE OPTIMIZATION PROBLEM

Suppose there are a total of m systems to draw evaluations from, including the real and the surrogates. Denote the output functions of these systems in increasing order of fidelity by $f_1(\mathbf{x}), f_2(\mathbf{x}), \ldots, f_m(\mathbf{x})$, where $\mathbf{x}$ is the input vector. Therefore, $f_1(\mathbf{x})$ has the lowest fidelity, and $f_m(\mathbf{x})$ has the highest fidelity. As mentioned previously, the highest-fidelity system is the system of interest, therefore the goal is to minimize $f_m(\mathbf{x})$ within the feasible region, χ, i.e.

$$\min_{x \in \chi} f_m(x) \quad . \tag{10}$$

We consider the systems as black boxes that provide no information other than measurements of the outputs. Denoting by d the dimension of the input space, we assume that the feasible region $\chi \subset R^d$ is connected and compact.

Each system is associated with a cost-per-evaluation, which is denoted by $C_1, C_2, \ldots, C_m$, respectively. In this research, the total cost of all evaluations measures the efficiency of the optimization scheme. Usually, a lower-fidelity evaluation is cheaper than a higher-fidelity evaluation, i.e., $C_1 < C_2 < \ldots < C_m$. Also, for now we assume that the cost of even the cheapest system is somewhat expensive, such that it is "worthwhile" to regenerate a radial basis function metamodel in order to determine the next search location.

In addition, the measurements of a system output may contain random error or noise. For each system, we assume that random errors from successive measurements are independent identically distributed (IID) normal deviates.

4.3.2 GENERAL OPTIMIZATION FRAMEWORK

The outline for the proposed Multiple Fidelity Sequential Radial Basis Optimization (MFSRBO) is as follows:

Step 1: Initialize radial basis function parameter(s), e.g., γ and the residual parameters, e.g., r, the number of computational analyses for residual or error estimation.

Step 2: Perform an initial experimental design involving all fidelity levels. Section 4.3.3 describes the options and focuses on n run Latin hypercube initial experiments following Huang, Allen, Notz, and Miller (2006).

4 also referred herein as "experimental run"

Step 3: Fit the radial basis function of the selected type (see Section 4.2.2) to all available data using singular value decomposition (SVD)-based least squares estimation.

Step 4: Find the location and fidelity level of the new evaluation that maximize the augmented expected improvement (EI) function. If the EI function is sufficiently small, go to Step 6.

Step 5: Conduct an evaluation at the selected point from Step 4. Go to Step 3.

Step 6: Perform an additional search and/or evaluation to evaluate solution quality. For example, apply trust region evaluation which includes a check for Karush-Kuhn-Tucker point convergence.

Note the removal of a diagnostic step from the Huang, Allen, Notz, and Miller (2006) because there is no need to assume zero expected mean for the biasing functions, δ_l. This constitutes one advantage of sequential radial basis optimization (MFSRBO) methods proposed here and may be expected to lead to relatively robust performance, particularly in cases involving large systematic errors.

By convention, Step 1 is also referred to as the "initial fit" stage, while Steps 4 and 5 are called the "infill" or "update" stage. The sequentially added evaluations are also called the "infill" or "update" points. Note that the proposed method differs from its predecessors mainly in the following two aspects: 1) the radial basis function metamodel is generated using multiple fidelity data, and 2) the EI formulation takes into account not only the location but also the fidelity level of an infill point.

4.3.3 DESIGN FOR INITIAL FIT

Step 2 in the previous section involves an experimental design for an initial fit. This is essentially the same as the initial step in methods based on Kriging models (e.g., Huang, Allen, Notz, and Miller 2006). Again, assume the number of factors is d. The methods in Huang, Allen, Notz, and Miller used an $n = 10 \times d$ run maximum minimum distance Latin hypercube (from the *lhsdesign* function in MATLAB®) for the lowest fidelity system and then selected a subset for higher fidelity systems. If the system includes random errors, d replicates are added to all levels at locations where the best responses are found.

As another alternative for future exploration, we suggest an initial design that includes all points on a grid for the lowest fidelity level. For each higher fidelity system, a subset of the previous points is selected including the q% of the best results from lower fidelity levels. In most of the numerical examples shown in this report, $q = 25\%$. The rational for using a grid instead of a Latin hypercube is that the projection properties of Latin hypercubes are likely not relevant since all systems are generally important. Also, radial basis functions are not affected by the numerical errors for Kriging models associated with equally spaced inputs.

4.3.4 EXPECTED IMPROVEMENT FUNCTIONS

The expected improvement function fits into the search framework in Section 4.3.2 and is used to select the next "infill" point. The function balances the desire to improve the search criterion with the desire to reduce uncertainty in a manner reminiscent of trust region point selection. The methods explored here are a straightforward application of the formulation in Huang, Allen, Notz, and Miller (2006) except that they are based on radial basis functions instead of Kriging models.

Therefore, for Multiple Fidelity Sequential Radial Basis Optimization (MFSRBO), we propose the following augmented Expected Improvement function:

$$EI(x,l) \equiv \underset{\varepsilon}{E}\left[\max\left(\hat{f}_m(x^*) - \hat{f}_m(x) - \sigma_m(x)\varepsilon, 0\right)\right]\alpha_1(x,l)\cdot\alpha_2(x,l)\cdot\alpha_3(l) \qquad \textbf{(11)}$$

where ε is normally distributed N[0,1] and

$$\alpha_1(x,l) = \text{ function that discounts systems relating to their predicted accuracy,} \qquad \textbf{(12)}$$

$$\alpha_2(x,l) = \left(1 - \hat{\sigma}_0 \,/\, \sqrt{\hat{\sigma}_l^2(x) + \hat{\sigma}_0^2}\right), \tag{13}$$

and $\alpha_3(l) = \dfrac{Cost_m}{Cost_l}$.

If the problem is deterministic, i.e., with zero repeatability error, then we (generally) use $\alpha_2(\mathbf{x},l) = 1$ and $\hat{f}_m(x^*)$ is the minimum of the already sampled points. More generally, if at least a single system has noise, in Eq. (11), **x*** stands for the current "effective best solution" defined by

$$x^* = \underset{x \in \{x_1, x_2, \ldots x_n\}}{\operatorname{argmax}} \left[u(x)\right] \tag{14}$$

where $u(x) = -\hat{f}_m(x) - \mu\,\hat{\sigma}_m(x)$. The formula from Jones, Schonlau, and Welch (1998) is:

$$\begin{aligned} &\underset{\varepsilon}{E}\left[\max\left(\hat{f}_m(x^*) - \hat{f}_m(x) - \sigma(x)\varepsilon, 0\right)\right] = \\ &\left(\hat{f}_m(x^*) - \hat{f}_m(x)\right)\boldsymbol{\psi}\left(\frac{\hat{f}_m(x^*) - \hat{f}_m(x)}{\hat{\sigma}_m(x)}\right) + \hat{\sigma}_m(x)\,\boldsymbol{\phi}\left(\frac{\hat{f}_m(x^*) - \hat{f}_m(x)}{\hat{\sigma}_m(x)}\right) \end{aligned} \tag{15}$$

where $\boldsymbol{\psi}$ is the cumulative normal and $\boldsymbol{\phi}$ is the normal density. We need the two formulas for the variance, i.e., with and without bias. In Huang, Allen, Notz, and Miller (2006), α_1 was chosen as

$$\alpha_1(x,l) = \operatorname{corr}\left[\hat{f}_m(x) + \epsilon_1\hat{\sigma}_m(x), \hat{f}_l(x) + \epsilon_2\hat{\sigma}_l(x)\right] \tag{16}$$

where "corr" is the correlation function and ϵ_1 and ϵ_2 are independent normally distributed deviates.

This choice had the following desirable properties:

1. It is easy to compute in the context of Kriging models,
2. When $l = m$, it equals 1.
3. For deterministic systems, it equals zero at past design points since $\sigma_l(\mathbf{x})$ is zero.

Unfortunately, for radial basis function systems, Eq. (16) is not easy to compute. In the "augmented dimensionality" version of our method, we inserted an estimate of Eq. (16) based on numerical integration (see Appendix A). For other methods, we used the following formulation which is relatively easy to compute:

$$\alpha_1(x,l) = \frac{\hat{\sigma}_l(x)}{|\hat{f}_m(x) - \hat{f}_l(x)| + \hat{\sigma}_m(x)} \tag{17}$$

where || is the absolute value. This approach has the above-mentioned desirable properties in the context of radial basis functions.

4.3.5 METHODS VARIATIONS

Every combination of modeling method, expected improvement function (assumed random error, simply estimated random errors, PRESS, and bias plus variance), expected improvement function (deterministic or stochastic), and termination sequence (simple or trust region) hypothetically corresponds to a method variation. Here, we consider only a select few combinations, characteristics of which are summarized in **Table 2**.

If the method has simple termination then it is called multifidelity sequential radial basis optimization (MFSRBO) or, for cases involving only a single level of fidelity, sequential radial basis optimization (SRBO). If the method terminates by applying a downhill search such as trust region augmented Lagrangian methods, then we refer to the method as a "hybrid".

Table 2. Variants considered in the computational and theoretical approach.

Method Variant	Prediction Uncertainty	EI Function	Termination
1. MFSRBO: augmented dimensionality	Variance Intervals based on assumed prediction errors	Deterministic	Simple
2. MFSRBO: cascading model	Variance intervals from estimated random errors	Deterministic	Simple
3. SRBO: cascading model	Variance intervals from estimated random errors	Stochastic	Simple
4. Hybrid	Variance intervals from estimated random errors	Both	Trust Region Augmented Lagrangian

4.3.6 COMPUTER CODES

The method "MFSRBO: augmented dimensionality" was used to demonstrate multifidelity radial basis function optimization on a real-world aerospace example (Section 5.2.3). This method was implemented using NEAR RS, a radial basis function-based regression tool whose response surface search module was modified to accommodate the computation of the multifidelity expected improvement function as the optimization driver. In NEAR RS the multifidelity cumulative metamodel concept relies formally on a dimensionality augmentation of the input data (control variables) space by including the fidelity level as an additional variable, Eq. (6). Search projections are required to counter this dimensionality augmentation and confine the optimization to the subspace corresponding to the desired level of fidelity. In other words, we seek to optimize a function (or its metamodel representation) on the high-fidelity manifold, regardless of where low-fidelity optima may be. The point of view adopted here is that the lower fidelity data act as "support" vectors aiding the characterization of the high-fidelity space.

NEAR RS's response surface search module is written in GNU Octave, an interpreter-based, Matlab®-like program for high level computation that is freely available under GNU General Public License. While very versatile, the associated code was not judged to be computationally efficient enough for widespread use. This is due in part to the nature of Octave, as opposed to the execution speed of a compiled language, such as ANSI C, and in part to the cost of computing numerically the correlation term (Appendix A) at each evaluation of the surrogate. Additional complications include the use of Options 1 and/or 2 (Section 4.2.2.3) for the modeling prediction variance, ascribing an inputed variance at each data point ("support" vector) according to what is believed to be a known or typical uncertainty associated with a particular code for a particular problem. This approach lacks rigor, because it ascribes an essentially epistemic type of uncertainty (i.e., no assumptions in regard to the distribution of the error within the interval), and subsequently treats this uncertainty as if it were aleatory uncertainty[5]. Furthermore, what could be principally bias error is treated as variance.

Thus, while the above methods have enjoyed empirical success, the *assumption* of the variance complicates comparison with methods that are not based on assumed random errors in Huang, Allen, Notz, and Zheng (2005) and Huang, Allen, Notz, and Miller (2006). Also, these alternative methods have explicit models for the systematic errors through their "cascading" model formulation and thus likely converge to a true picture of the fidelity hierarchy. For this reason, the comparison results presented in Section 5.2.2 are based on method variants 2-3 (SRBO: cascading models and MFSRBO: cascading models) and were implemented in a new code, the features of which include:

[1] The ability to call Windows simulation and read results using shell and wait,

[2] Enumeration-based (inefficient but repeatable) expected improvement function optimization (every iteration, the code evaluates all alternatives on a grid to select the point that maximizes the expected improvement), and

[3] Microsoft excel interface.

5 In other words, the input uncertainty internal is treated as the standard error of a stochastic process.

The code developed for these purposes is a combination of ANSI C++ and Visual Basic (VB). The developed code is not owned or copyrighted by any participants not on the Team. The singular value decomposition (SVD) estimation code was based on numerical recipes code which was significantly altered. The hybrid designs considered here are only for the convergence results established in the next section. Additional hybrid designs are proposed for future research to offer improved computational results while achieving rigorous convergence.

4.4 COMPUTATIONAL ANALYSIS METHODS

The computational results presented in this report (Section 5.2) consist of several test problems (e.g., Branin function, multifidelity Rosenbrock function) and two applications involving computational structural and computational fluid modeling.

For the structural analysis tool we used McIntosh Structural Dynamics' finite element code CNEVAL (Lesieutre et al., 1997). The wing structure was modeled using conformal quadrilateral plate elements cantilevered at the root chord. Given the normal aerodynamic forces, CNEVAL provides the structural displacements, stresses, frequencies, and overall structural weight. CNEVAL was used to predict the static aeroelastic deformations and to verify that structural limits were not exceeded. CNEVAL uses the current wing planform information,[6] along with the planform thickness information and material properties, and updates the finite-element model of the wing which is subdivided into quadrilateral panels used to distribute the aerodynamic loads for the wing displacement calculations. Each panel is divided into 2 triangles. An option also exists to further subdivide a quad element into 4 triangles for greater accuracy. Both high- and low-fidelity structural modeling were carried out using CNEVAL by changing the finite element discretization, as described in **Table 3**.

Table 3. Finite element discretization.

Wing Design Problem	Fidelity Level	Number of Structural Elements		Element Type
		Chordwise	Spanwise	
Unswept tapered	High	10	15	4 triangle elements per structural quad
	Low	2	2	2 triangle elements per structural quad
UAV, swept	High	10	15	2 triangle elements per structural quad
	Low	4	7	2 triangle elements per structural quad

A version of NEAR's intermediate-level aerodynamic prediction code MISDL (Lesieutre et al., 1998, Dillenius et al., 1999) was used as the high-fidelity fluid model. MISDL is based on panel methods, vortex lattice with compressibility correction for subsonic flow, and other classical singularity methods enhanced with models for nonlinear vortical effects. The method is applicable to subsonic and supersonic flight vehicles including aircraft, UAVs, missiles, and rockets. Circular and noncircular cross section bodies are modeled by either subsonic or supersonic sources/sinks and doublets for volume and angle of attack effects, respectively. Conformal mapping techniques are used for noncircular bodies. The fin/wing sections are modeled by a horseshoe-vortex panel method for subsonic flow and by first-order constant pressure panels for supersonic flow. Up to three lifting surface sections can be modeled and nonlinear fin and body vortices are modeled. MISDL predicts overall aerodynamic performance coefficients and detailed aerodynamic loading distributions. The code has seen extensive use in missile aerodynamic analysis and design, including aerodynamic shape optimization and multidisciplinary design optimization when coupled to a structural finite element model. In recent years, MISDL has seen use in the analysis of manned and unmanned (UAV) aircraft.

OPTMIS is the name used to designate the version of MISDL that is coupled with CNEVAL.[7] The cross-disciplinary coupling is handled by the OPTMIS logic through successive iteration between codes. OPTMIS handles interpolation, displacement and load transfer operations and iterates between

6 i.e., the (x,y)-projected shape of the wing

7 OPTMIS also contains an optimization module of its own, based on Powell's conjugate gradient method, but the optimization component was not used in this study.

aerodynamic and structural predictions until a prescribed convergence level is reached. Convergence is obtained when the change in the displacements between successive iterations is less than a user-prescribed threshold at all structural node points. For the purposes of this study, OPTMIS was enhanced with the computation of the induced drag. Rather than incorporating a Trefftz plane analysis, such as might be done in an Euler code, the induced drag was computed using a direct method, as follows.

To compute the induced forces on the wing, the Kutta-Joukowski theorem is used: $\vec{F}_i = \rho \vec{u}_i \times \vec{\Gamma}_i$. This induced force vector is computed on each panel as the cross product of the total induced velocity on the panel (sum of all vortex lattice induced velocities; the freestream velocity being omitted) and the panel bound vortex vector. The drag component of $\vec{F}_i$ from each panel is computed and summed to obtain the total induced drag. Several test cases were used to verify the calculation, and the theoretical limit of $C_{Di} = C_L^2/(\pi AR)$ was obtained for elliptically loaded wings. An option also exists to prescribe a cosine-shaped spanwise layout of the panels[8] to increase computational accuracy. The low-fidelity fluid modeling amounted to simple lifting line theory, conveniently implemented within OPTMIS using a degenerate panel layout, as shown in **Table 4**. Code robustness issues precluded the use of this implementation for the case of the UAV wing planform and, so, for this case, the low-fidelity model consisted of a coarse panel discretization aerodynamic model, the details of which are also furnished in **Table 4**.

Table 4. Aerodynamic Panel Layout.

Wing Design Problem	Fidelity Level	Number ofAerodynamic Panels		Spanwise Panel Layout
		Chordwise	Spanwise	
Unswept tapered	High	10	15	Cosine distribution
	Low	1	2	Uniform
UAV, swept	High	10	15	Uniform
	Low	4	7	Uniform

The isotropic material used for the structure was aluminum. We used the following material constants:

Table 5. Material Properties.

Material Property	Value
Young's modulus	10.5×10^6 lbf/in^2
Poisson's ratio	0.3
Density	0.1 lb/in^3
Maximum allowed Von Mises stress	22.5×10^3 lbf/in^2

The structural cross section geometry was self-similar as a function of span, and idealized as shown in **Figure 2**. All parameters in **Figure 2** were modeled as being linearly varying from root to tip, with maximum and minimum values indicated in **Table 6**.

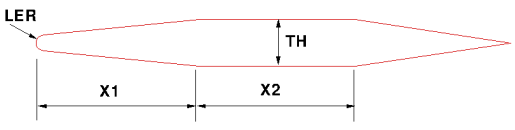

Figure 2. Structural cross-section.

Table 6. Geometric Parameters (in ft.).

Geometric Parameters	Tapered wing	UAV wing
X1_root	0.2	0.348
X2_root	0.3	0
TH_root	*variable*	0.025
X1_tip	0.2	0.103
X2_tip	0.3	0
TH_tip	0.028	0.025
LER	0	0

8 exhibiting maximum refinement at the wing tip

5. RESULTS

The results of this STTR Phase I are organized as follows. Convergence results are first presented, followed by computational results. The computational results include comparisons between methods based on single fidelity level results (Section 5.2.1), application of multifidelity optimization to model problems (Section 5.2.2), and multifidelity multidisciplinary design problems involving aeroelastic wings.

5.1 RIGOROUS CONVERGENCE RESULTS

This section describes rigorous convergence of the methods that we call "hybrid" methods (see Section 4.3.5). The convergence proof is obvious and builds on the multifidelity convergence results from Rodriguez, Renaud, and Watson (1998). Those authors described rigorous results and showed that their trust region method converged under the assumptions they defined. Their results hold for deterministic optimization only and are typical perhaps of nonlinear programming convergence to local minima results. In general, with only a few conditions any downhill search converges. The contribution here relates to the multifidelity aspect of the modeling.

After clarifying their conditions and the trivial convergence of hybrid methods we discuss how some of the Rodriguez, Renaud, and Watson (1998) conditions might be relaxed and computationally efficient methods might be developed with rigorous guarantees. The hybrid methods are assumed to be likely to offer global results similar to other methods based on global methods and convergence similar to trust region methods. Yet, it is believed further method development will be needed to achieve both global and rigorous convergence results and the computational efficiency of nonhybrid methods.

5.1.1 CONVERGENCE CONDITIONS

Trust region augmented Lagrangian multifidelity methods have been proven to converge to local optima of the highest fidelity system (Rodriguez, Renaud, and Watson, 1998). Yet, their assumptions include that the systems are deterministic and that the fidelity level, ψ, can be continuously adjusted. In the context of multiple local minima they can be considered inferior since sequential optimization methods using global metamodels have been demonstrated on test problems to converge efficiently to the global optimum.

The purpose of this section is to clarify the conditions used to prove the trust region convergence. As a result, reviewing the assumptions from Rodriguez, Renaud, and Watson (1998) clarifies the convergence criteria for hybrid methods. It also illuminates the conditions and issues for future, more efficient hybrid optimization method convergence. Because the notation used is somewhat different than in preceding sections and because of the length of the material, the list of underlying assumptions is relegated to Appendix B.

5.1.2 CONVERGENCE RESULTS

Clearly, if a method can be applied starting at any point and converge, convergence is guaranteed starting from the output of a SRBO or MFSRBO method. Therefore, simple hybrid methods converge if the method used in the last phase converges.

Nontrivial combinations of sequential radial basis optimization (SRBO) and trust region components can certainly be developed that offer computational efficiency advantages and proven convergence benefits. The key issues are the issues for virtually all nonlinear programming methods: (1) maintaining of positive probability of improvement and (2) converging only when the conditions for a local minimum (KKT) are met. Also, the proofs in Rodriguez, Renaud, and Watson (1998) are presented in terms of a series of paired levels of fidelity. It seems likely that the key steps can be revised so that the fidelity levels can be discrete and the proof still applies.

5.2 COMPUTATIONAL RESULTS

The MFSRBO algorithm outlined above was developed, tested, and refined based on a numerical test bed consisting of eight different optimization problems. The main characteristics of these eight problems are outlined in **Table 7**.

Table 7. Overview of numerical test cases.

Test Problem Name		Goal / Comment	Multi-Disciplinary	Multi-Fidelity	Design Variables	Number of Constraints: Aero.	Number of Constraints: Structural
Six hump Branin function		Unconstrainted minimization, exhaustive grid-based search, comparison to other methods	no	no	x_1, x_2	n/a	
Rosenbrock function & approximation		Unconstrainted multifidelity minimization	no	✓	x_1, x_2	n/a	
Symmetrized Rosenbrock function & approximation		Multifidelity optimization with two distinct optima	no	✓	x_1, x_2	n/a	
Aeroelastic Wing Design	1	Minimize induced drag, subject to lift and stress constraints	✓	✓	α_0	1	1
"	2				α_0, $d\alpha/ds$	1	1
"	3				α_0, $d\alpha/ds$, θ_0	1	1
"	4				α_0, $d\alpha/ds$, θ_0, Λ	1	1
UAV Aeroelastic Wing Design		Optimize stability, subject to trim, payload, and stress constraints	✓	✓	α_0, $d\alpha/ds$	2	1

With the exception of the first test problem (Section 5.2.1), the surrogate search used in each of the optimizations amounts to a multistart steepest ascent[9] scatter-and-poll strategy (Queipo et al., 2005) for calculating $arg\left(max\left(EI(\boldsymbol{x},1)\right)\right)$.

5.2.1 SINGLE FIDELITY LEVEL RESULTS

The single fidelity results presented in this section are almost the same for the test functions the OSU members of our Team considered as the results in Huang, Allen, Notz, and Miller (2006) and Huang, Allen, Notz, and Zheng (2006). This follows because in virtually all of the test problems good solutions were obtained from the initial design portions which were identical between the Kriging model and radial basis function-based approaches. In all of the problems in Huang, Allen, Notz, and Miller (2006), for example, fewer than 25% of the evaluations were after the initial design evaluations. First, we consider the single fidelity noisy case for simplicity.

In the results shown below the Sequential Radial Basis Optimization (SRBO) method is empirically compared with three alternative approaches from the literature. The first alternative considered is the Simultaneous Perturbation Stochastic Approximation (SPSA) from Spall (1998). The second approach is the Revised Simplex Search (RSS) procedure, a variant of the Nelder-Mead method, proposed by Humphrey and Wilson (2000). As the original RSS procedure was not designed to handle constraints, we modify it so that whenever a point is infeasible, the algorithm selects the

9 see Appendix A for further detail

nearest feasible point instead. The third approach is the DIRECT method developed by Gablonsky (2001) et al.

Here, we focus on a single fidelity system with noise. In this case, the test function is the six hump camelback function from Branin (1972) with ~ N(0, 0.122) noise added. The function is:

$$f(x) = 4\,x_1^2 - 2.1\,x_1^4 + 1/3\,x_1^6 + x_1\,x_2 - 4\,x_2^2 + 4\,x_2^4 \qquad \textbf{(18)}$$

$$-1.6 \le x_1 \le 2.4,\ -0.8 \le x_2 \le 1.2$$

$$\mathbf{x}^* = (0.089, -0.713) \text{ and } (-0.089, 0.713),\ f^* = -1.03$$

In this problem, there are six local and two global optima. For the single fidelity, noisy case, the expected improvement function (Eq. (11)) simplifies with $\alpha_1 = \alpha_3 = 1$.

Figure 3 plots two randomly selected sequential radial basis optimization (SRBO) runs overlaid on the results of four alternative methods. The SRBO method was applied using $\gamma = 0.5$ and $r = 3$, i.e., the last three runs are used for the residual. The results indicate that SRBO methods converge quickly like sequential Kriging optimization (SKO) methods. There might be an issue with convergence although that might relate to the 100×100 grid used for expected improvement optimization. It is also possible that the convergence is limited by the constant γ, which explains why our Team varied γ in our aerospace wing case study (Section 5.2.3).

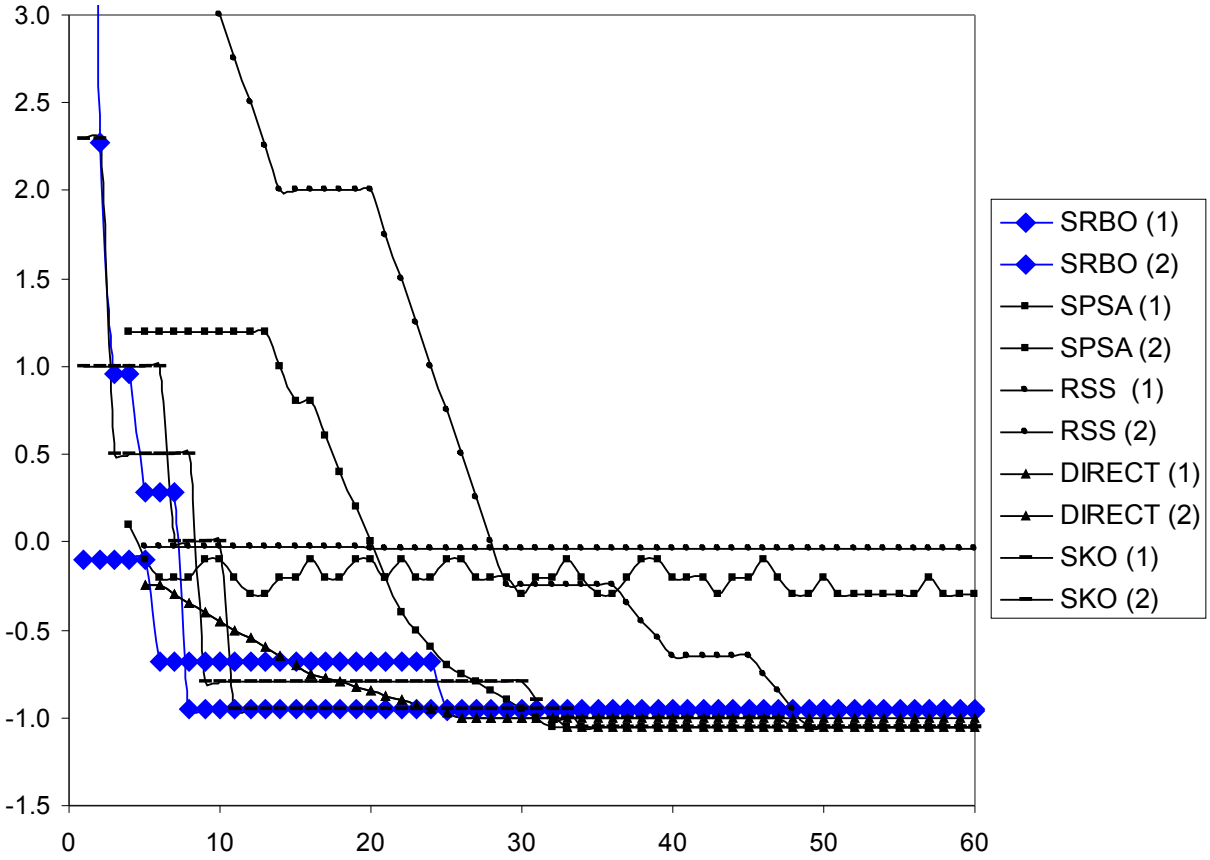

Figure 3. Results from two randomly selected runs of each method on the six hump camel back function. (Vertical axis corresponds to the function value. Horizontal axis corresponds to the number of function calls).

5.2.2 MULTIFIDELITY TEST PROBLEM

The application of the augmented dimensionality multifidelity sequential radial basis optimization (MFSRBO) to Rosenbrock's function is considered next. Similarly to Eldred et al. (2004), we consider the minimization of Rosenbrock's function (**Figure 4**):

$$f_{HF} = 100(x_2 - x_1^2)^2 + (1 - x_1)^2 \quad \textbf{(19)}$$

f_{HF} is the true (high-fidelity) function to be minimized. It's low-fidelity surrogate f_{LF} is defined as

$$f_{LF} = 100(x_2 - x_1^2 + 0.2)^2 + (0.8 - x_1)^2 \quad \textbf{(20)}$$

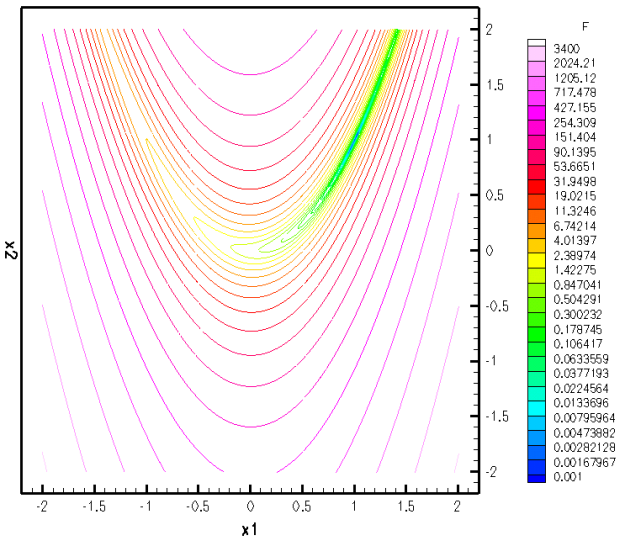

Figure 4. Isocontours of the high-fidelity Rosenbrock function.

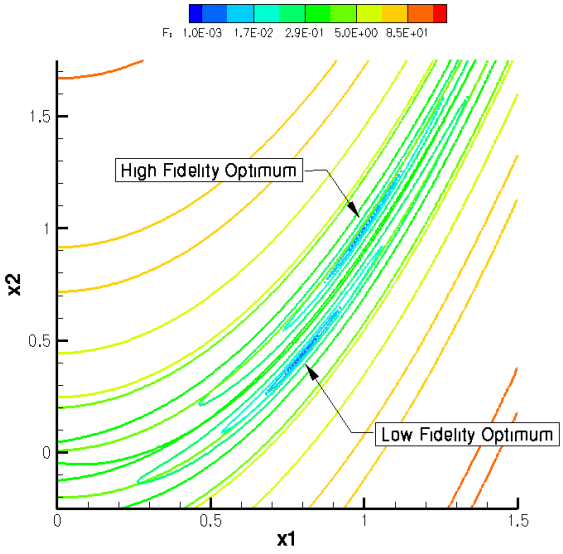

Figure 5. Comparison between the Rosenbrock function and its low-fidelity counterpart in the vicinity of their optima.

While the two functions have similar structure, the high-fidelity function has its minimum at ($x_1 = 1$, $x_2 = 1$), the low-fidelity one at ($x_1 = 0.8$, $x_2 = 0.44$). The two functions are not, in the strictest sense, weakly consistent, but the problem has favorable structure. In the immediate vicinity of the high-fidelity optimum $f_{HF} = 0$ but $f_{LF} \approx 4$ and the difference between the two models exhibits strong gradients, as illustrated in **Figure 5**.

Because the methods described in Section 4.2.2 integrate data at all levels of fidelity to build a global radial basis function metamodel, it is possible to use the associated Multifidelity Expected Improvement function (Eq. (11)) as the criterion determining the location and fidelity level of subsequent evaluations:

$$EI(\boldsymbol{x}, k) \overset{\text{def}}{=} E\left[max\left(\hat{f}_m(\boldsymbol{x}^*) - \hat{f}_m(\boldsymbol{x}) - \sigma_m(\boldsymbol{x})\epsilon, 0\right)\right].corr\left[\hat{f}_k(\boldsymbol{x}), \hat{f}_m(\boldsymbol{x})\right].\left(1 - \frac{\hat{\sigma}_{0,k}}{\sqrt{\hat{\sigma}_k^2(\boldsymbol{x}) + \hat{\sigma}_{0,k}^2}}\right).\frac{Cost_m}{Cost_k}$$

where $\hat{f}_m(\boldsymbol{x})$ is the high-fidelity prediction at point $\boldsymbol{x}$, and $\boldsymbol{x}^*$ is the current "effective best solution" defined in Eq. (14). $\hat{\sigma}_{0,k}^2$ is the unexplained variance of the radial basis function model at level k, and $\hat{\sigma}_k^2(\boldsymbol{x})$ is the variance of $\hat{f}_k(\boldsymbol{x})$. The correlation term $corr\left[\hat{f}_k(\boldsymbol{x}), \hat{f}_m(\boldsymbol{x})\right]$ is used to discount the expected improvement when an evaluation from a lower fidelity surrogate is used. The term involving $\hat{\sigma}_{0,k}^2$ accounts for diminishing returns of additional replicates as the prediction becomes more accurate, and the cost ratio adjusts the sampling strategy according to the evaluation costs (Huang et al., 2006). The location and fidelity of the next evaluation, $\boldsymbol{x}_{n+1}$ and k_{n+1} are given by maximizing $EI(\boldsymbol{x}, k)$, i.e.:

$$(\boldsymbol{x}_{n+1}, k_{n+1}) = arg\left(max\left(EI(\boldsymbol{x}, l)\right)\right) \tag{21}$$

The effective best solution $\boldsymbol{x}^*$ is defined by $\boldsymbol{x}^* = arg\left(max\left(u(\boldsymbol{x})\right)\right)$ where $u(\boldsymbol{x}) = -\hat{f}_m(\boldsymbol{x}) - \mu s_m(\boldsymbol{x})$ expresses the willingness to trade one unit of the predicted objective for μ units of the standard deviation of the prediction uncertainty (Schenk et al., 2005). Also, the expectation in $EI(\boldsymbol{x}, k)$ is conditional given the past data and given estimates of the correlation parameters. Thus, the expectation is computed by integrating over the distribution of $\hat{f}_m(\boldsymbol{x})$, with $\hat{f}_m(\boldsymbol{x}^*)$ fixed. Specifically, assuming a normally distributed error, the *probability of improvement* $P[\hat{f}_m(\boldsymbol{x}) < \hat{f}_m(\boldsymbol{x}^*)]$ is defined as

$$P[\hat{f}_m(\boldsymbol{x}) < \hat{f}_m(\boldsymbol{x}^*)] = \frac{1}{s_m(\boldsymbol{x})} \int_{-\infty}^{\hat{f}_m(\boldsymbol{x}^*)} \boldsymbol{\phi}(y - \hat{f}_m(\boldsymbol{x}); s_m(\boldsymbol{x}))\, dy \tag{22}$$

where $\boldsymbol{\phi}$ is the probability density function:

$$\boldsymbol{\phi}(y; \sigma) = \frac{1}{\sqrt{(2\pi)}} \exp\left(-\frac{y^2}{2\sigma^2}\right) \tag{23}$$

As pointed out in Forrester et al. (2009), the *expected improvement* is the first moment of Eq. (22), i.e.,

$$EI\,|_{\hat{f}_m(\boldsymbol{x}) < \hat{f}_m(\boldsymbol{x}^*)} = \frac{1}{s_m(\boldsymbol{x})} \int_{-\infty}^{\hat{f}_m(\boldsymbol{x}^*)} (\hat{f}_m(\boldsymbol{x}) - y).\boldsymbol{\phi}(y - \hat{f}_m(\boldsymbol{x}); s_m(\boldsymbol{x}))\, dy \tag{24}$$

After integration by parts, the expectation can be calculated analytically as follows:

$$\begin{aligned} E\left[\max\left(\hat{f}_m(\boldsymbol{x}^*) - \hat{f}_m(\boldsymbol{x}), 0\right)\right] &= \left(\hat{f}_m(\boldsymbol{x}^*) - \hat{f}_m(\boldsymbol{x})\right).\boldsymbol{\psi}\left(\hat{f}_m(\boldsymbol{x}^*) - \hat{f}_m(\boldsymbol{x}); s_m(\boldsymbol{x})\right) \\ &+ \quad s_m(\boldsymbol{x}).\boldsymbol{\phi}\left(\hat{f}_m(\boldsymbol{x}^*) - \hat{f}_m(\boldsymbol{x}); s_m(\boldsymbol{x})\right) \end{aligned} \tag{25}$$

where $\boldsymbol{\phi}$ is the normal probability density function defined above, and $\boldsymbol{\psi}$ is the normal cumulative distribution function:

$$\boldsymbol{\psi}(y; \sigma) = \frac{1}{2}\left[1 + erf\left(\frac{y}{\sqrt{2}\sigma}\right)\right] \tag{26}$$

For the multifidelity Rosenbrock function, the initial design consisted of four points (the four corners in **Figure 4**), three of which were low-fidelity. The high-fidelity corner was chosen randomly. An assumed data point uncertainty (σ_0 in Eq. (8)) of 0.01 was used.[10] A typical optimization result is shown in **Figure 6** which depicts the search path history. In **Figure 6** the low-fidelity function evaluations are identified by the small symbols and the high-fidelity ones with the larger symbols.

The optimization correctly identifies the high-fidelity optimum in a relatively small number of high-fidelity function evaluations. For reference, **Figure 7** shows the low-fidelity subset of **Figure 6**, super-imposed on isocontours of the low-fidelity function. This picture helps understand the role of the low-fidelity evaluation as an aid to sample the design landscape. Note in particular the accumulation of points near the high-fidelity optimum ($x_1 = 1$, $x_2 = 1$), not the low-fidelity one ($x_1 = 0.8$, $x_2 = 0.44$).

In the results depicted in **Figures 6** and **7** the assumed cost ratio between the two fidelity levels was 3/2. As expected, the multifidelity expected improvement function effectively drives the objective towards the high-fidelity optimum and takes advantage of the presumed-low-cost, low-fidelity evaluations to find a positive direction of improvement. The approach is successful because the cumulative radial basis function metamodel is able to "learn" the relationship between the low- and high-fidelity projections. In an ideal sense, this nonlinear relationship must be accurately defined using as few (expensive) high-

10 for purposes of comparison with the Branin function example considered in the previous section, this data point uncertainty can be thought of as ~ N(0, 0.01) "virtual" noise

fidelity observations as possible. Our empirical observations suggest that, because the uncertainty on this relationship remains large if the number of high-fidelity observations is too few, there is a practical tradeoff which must be considered in the initial design. For the majority of our experiments, the ratio of high-fidelity to low-fidelity initial count was around 25%.

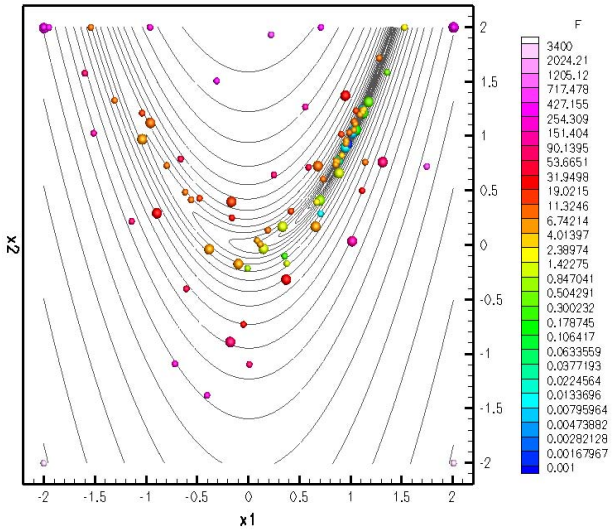

Figure 6. Multifidelity search path and isocontours of the high-fidelity Rosenbrock function.

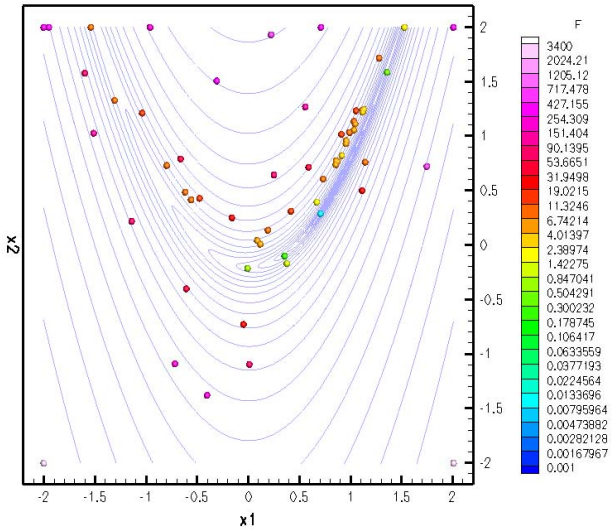

Figure 7. Low-fidelity subset of multifidelity search path with isocontours of the low-fidelity Rosenbrock function.

To further demonstrate the method on a problem exhibiting more than one local optimum, we considered the following dual optimum problem, constructed by smooth-symmetrizing the Rosenbrock function about the origin as follows:

$$h(x_1, x_2) = \eta \,.\, f(x_1, x_2) + (1-\eta) \,.\, f(-x_1, -x_2)$$
$$\eta = \frac{1}{2}\left(\tanh[20(x_1+x_2)]+1\right) \qquad \textbf{(27)}$$

In Eq. (27) f designates either f_{HF} or f_{LF} as appropriate.

As in the previous example, the initial design consists of the four corner points ($x_1 = \pm 2$, $x_2 = \pm 2$), only one of which is evaluated at the high-fidelity level.

Figure 8 shows the multifidelity search path obtained by MFSRBO with an assumed 3/2 cost ratio and an assumed $\sigma_0 = 0.01$. As in **Figure 6**, the small symbols in the figure represent the results of low-fidelity analyses, and the large symbols correspond to high-fidelity analyses. It is noteworthy that, regardless of the fidelity at which they are calculated, the accumulated designs find both optima of the *high-fidelity* function, h_{HF} .

The convergence history is illustrated in **Figure 9**, which depicts in semi-log scale the values $h_{HF}(x_1, x_2)$ of the high-fidelity infills in order of appearance. In order for the optimization to be able to both *explore* the design landscape and *exploit* the narrow minima, it is advantageous to relax the metamodel stiffness (i.e., increase γ (Section 4.2.2.1) or γ_i (Section 4.2.2.2)) as the design progresses. It its present implementation, this adaptivity is based on a simple, heuristic algorithm. This algorithm increases the γ_i parameters by a small factor

$$\gamma_i^{NEW} = (1+\tau_1)\gamma_i^{OLD} \qquad \textbf{(28)}$$

anytime the rank of the linear model design matrix **X** recedes below a given percentage of its full rank:

$$\frac{\text{rank}(\boldsymbol{X})}{n} \le \tau_2 \qquad \textbf{(29)}$$

For example, the results of **Figures 8** and **9** were obtained using $\tau_1 = 0.11$ and $\tau_2 = 0.94$.

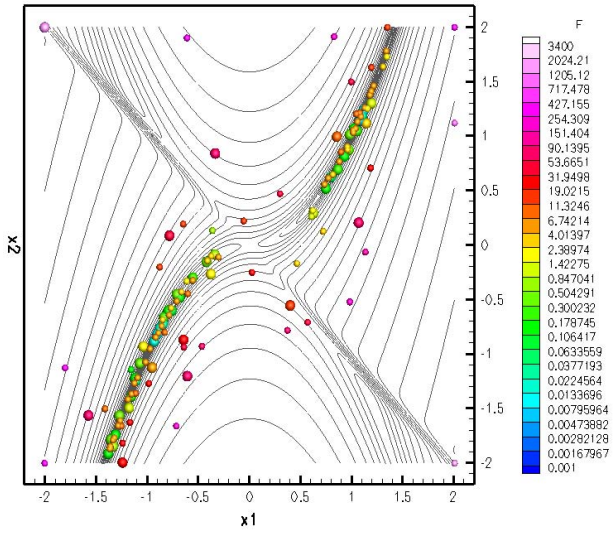

Figure 8. Multifidelity search path superimposed with isocontours of the high-fidelity symmetrized Rosenbrock function.

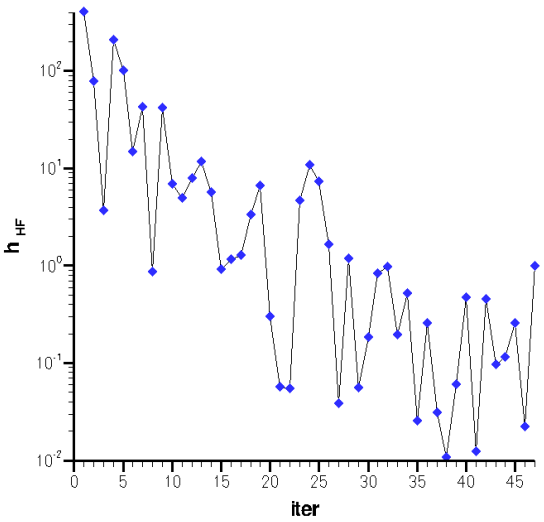

Figure 9. History of high-fidelity infills corresponding to the mulitifidelity optimization search path shown in **Figure 8**.

5.2.3 AEROELASTIC WING DESIGN PROBLEM

Two aeroelastic wing design problems were considered as part of this investigation. The first, designated "baseline problem," consisted of an aspect ratio 10 unswept rectangular or slightly tapered wing designed for minimal drag under load. The second problem, referred to as the "UAV wing design," was aimed at maximizing stability and was characterized by the incorporation of multiple constraints and a noisy objective function.

5.2.3.1 Baseline problem

A baseline problem was defined for the purpose of developing and demonstrating the MFSRBO approach and its ability to represent and integrate information from each discipline and model. Computational fluid dynamics (CFD) and computational structural mechanics (CSM) were initially targeted as examples of high-fidelity models for the two interacting disciplines (fluids and structures). However, the practical realities of the Phase I time frame and budget focused our attention instead on the following analysis methods and fidelity levels (see Section 4.4):

Table 8. Overview of computational methods used.

MODELS	Fluids	Structures
High Fidelity	OPTMIS/MISDL (NEAR), intermediate-level aerodynamic prediction code based on panel methods and other classical singularity methods enhanced with models for nonlinear vortical effects. Applicable to subsonic and supersonic flight vehicles including aircraft, UAVs, missiles, and rockets.	CNEVAL FEM method; provides weights, displacements, stresses, and modal frequencies
Low Fidelity	Lifting line theory, supplemented with induced drag calculation.	Low degree-of-freedom version of the CNEVAL FEM model.

An analysis of baseline problem candidates led to the selection of the minimum drag design of a wing subject to minimum lift and static aeroelastic constraints as the focus of the Phase I demonstration. This benchmark problem is derived from Robinson et al. (2006). It seeks to minimize the induced drag $C_{D,i}$ by changing the pre-load twist distribution (parameterized here by the root chord angle of attack α_0 and its spanwise first and second derivatives, $d\alpha/dy$ and $d^2\alpha/dy^2$). Two additional variables are introduced: the root chord maximum structural thickness $\theta_0 \triangleq \text{TH}(y=0)$, and the taper ratio $\Lambda \triangleq c_{tip}/c_{root}$ of the unswept flexible wing. The wing span is maintained constant, $y_{max} = 5\ ft$, and the wing area is kept fixed at $S = 5\ ft^2$.

The induced drag was minimized, subject to minimum lift and maximum stress constraints as follows:

$$\begin{aligned} &\text{minimize} && C_{D,i} \\ &\{\alpha_0, d\alpha/dy, \theta_0, \Lambda\} && \\ &\text{subject to} && C_L \geq (W_{payload} + W_{wing})/(q_\infty S_{ref}) \\ & && \sigma_{VM} / \sigma_{VM,max} < 0.5 \end{aligned} \qquad \textbf{(30)}$$

where σ_{VM} is the Von Mises stress, W is weight, q_∞ is dynamic pressure, and S_{ref} is the wing reference area. For this investigation, the freestream angle of attack is zero, the freestream Mach number is $M_\infty = 0.2$, the dynamic pressure is $q_\infty = 40.76\ psf$, and the assumed payload is $W_{payload} = 75\ lbs$.

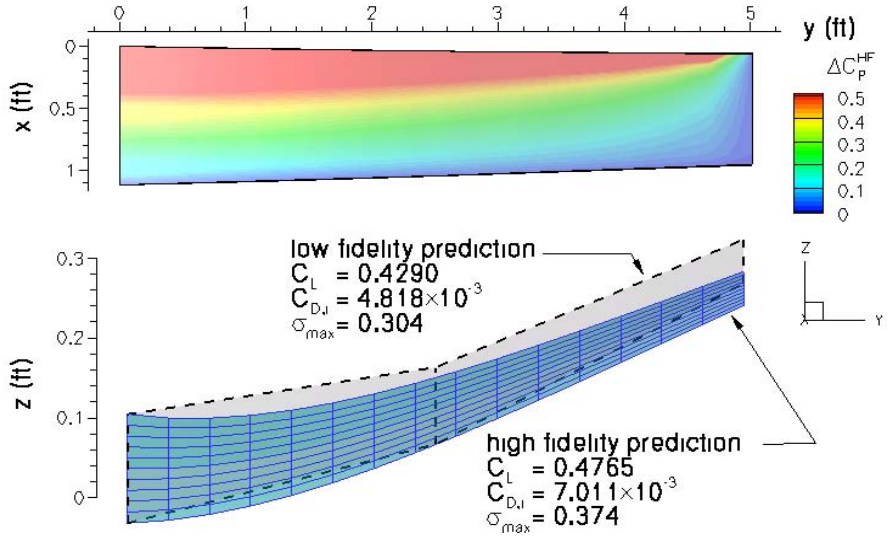

Figure 10. Low- and high -fidelity static aeroelastic deformation prediction. (Top: aerodynamic loading (planform view). Bottom: streamwise view of combined wing twist and bending (not to scale)).

A typical comparison of low- and high-fidelity analyses[11] is given in **Figure 10**,[12] corresponding to $\alpha_0 = 7^o$, $d\alpha/dy = -0.8^o\ ft^{-1}$, $d^2\alpha/dy^2 = 0^o\ ft^{-2}$, $\theta_0 = 0.045\ ft$, and $\Lambda = 0.8$ using the material and cross-sectional properties shown in Section 4.4.

One-, two-, three-, and four-dimensional variations on the minimum drag aeroelastic wing design problem were investigated as part of this effort. To better understand how the optimization method performed on these cases, let us consider the two-dimensional results (**Table 7**, subcase 2) in which a fixed root chord maximum thickness $\theta_0 = 0.04\ ft$ and fixed taper ratio $\Lambda = 1$ are used.

11 The cost ratio between high- and low-fidelity analyses was 5:1

12 "σ" in Figure 10 denotes the ratio $\sigma_{VM}/\sigma_{VM,max}$

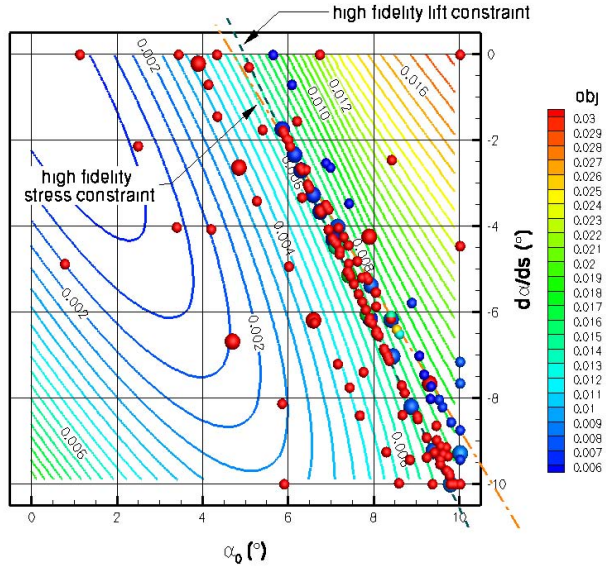

Figure 11. Sample multifidelity search path for two-dimensional aeroelastic wing design problem.

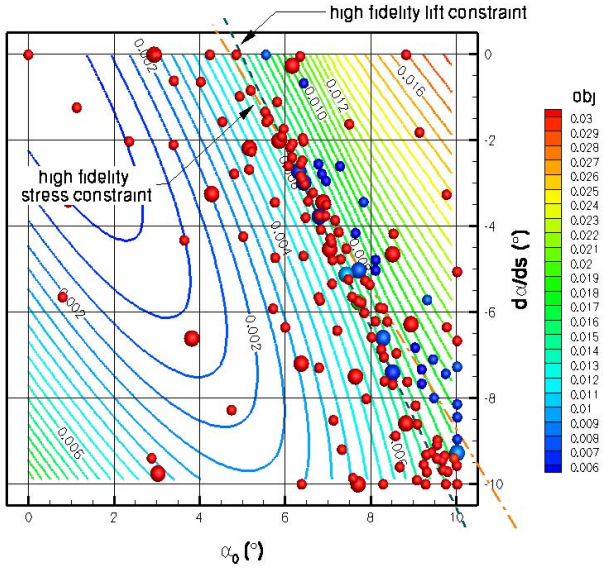

Figure 12. A different instantiation of the problem solved in **Figure 11** (different initial conditions).

Figures 11 and **12** provide two examples of the MFSRBO search path when the optimization is initiated from two randomly chosen Latin Hypercube design of experiments, each including one high-fidelity and three low-fidelity solutions (see **Table 9**).

Table 9. Listing of initial conditions

Point Number	Initial Design Used in Figure 11			Initial Design Used in Figure 12		
	α_0 (°)	$d\alpha/ds$ (°)	Fidelity level	α_0 (°)	$d\alpha/ds$ (°)	Fidelity level
1	8.405	-2.453	Low	**3.021**	**-9.752**	**High**
2	0.784	-4.876	Low	7.487	-1.617	Low
3	**4.690**	**-6.679**	**High**	9.019	-6.821	Low
4	5.851	-8.127	Low	0.934	-3.438	Low

The following computational analysis uncertainties (σ_0 in Eq. (8)) were used uniformly for the OPTMIS outputs:

Table 10. OPTIMS output uncertainties

	C_L	$C_{D,i}$	W_{wing} (lb)	$\sigma_{VM}/\sigma_{VM,max}$
σ_0	0.0002	0.002	0.03	0.02

The results of **Figures 11** and **12** are shown as a function of the two design variables α_0 and $d\alpha/ds$, where s is the nondimensional span variable, $s = y/y_{max}$. The background contour lines represent the high-fidelity primary (unconstrained) objective, $C_{D,i}$. The large symbols denote high-fidelity analyses, while the small symbols represent the low-fidelity analyses. Each symbol is colored based on the objective function, which is the induced drag $C_{D,i}$, modified with penalty functions for violating lift and/or stress constraints (themselves indicated by dashed lines). Specifically, the constraints are incorporated into the objective function using the following penalty formulation (using the previous values for W_{payload}, q_∞ and S_{ref}):

$$f = C_{D,i} + 10.\max\left[\left(\frac{75+W_{wing}}{40.76\times 5}\right) - C_L, 0\right] + 20.\max\left[\frac{\sigma_{VM}}{\sigma_{VM,max}} - 0.5, 0\right] \qquad \textbf{(31)}$$

where W_{wing} is the structural weight of the wing, expressed in pounds. The process of maximizing the multifidelity expected improvement function **(11)** involves calculating **(15)**, which requires keeping track of the current best effective solution $\boldsymbol{x}^* = [\alpha_0^*, (d\alpha/dy)^*, \theta_0^*, \Lambda^*]$, and the ability to estimate the objective function f and its variance s^2 at any design point $\boldsymbol{x}$ for any level of fidelity.

A more elegant way of handling the constraints in a consistent and fully probabilistic manner is described in Forrester et al. (2009). The detailed implementation of this method applied to the present problem is described in Appendix C.

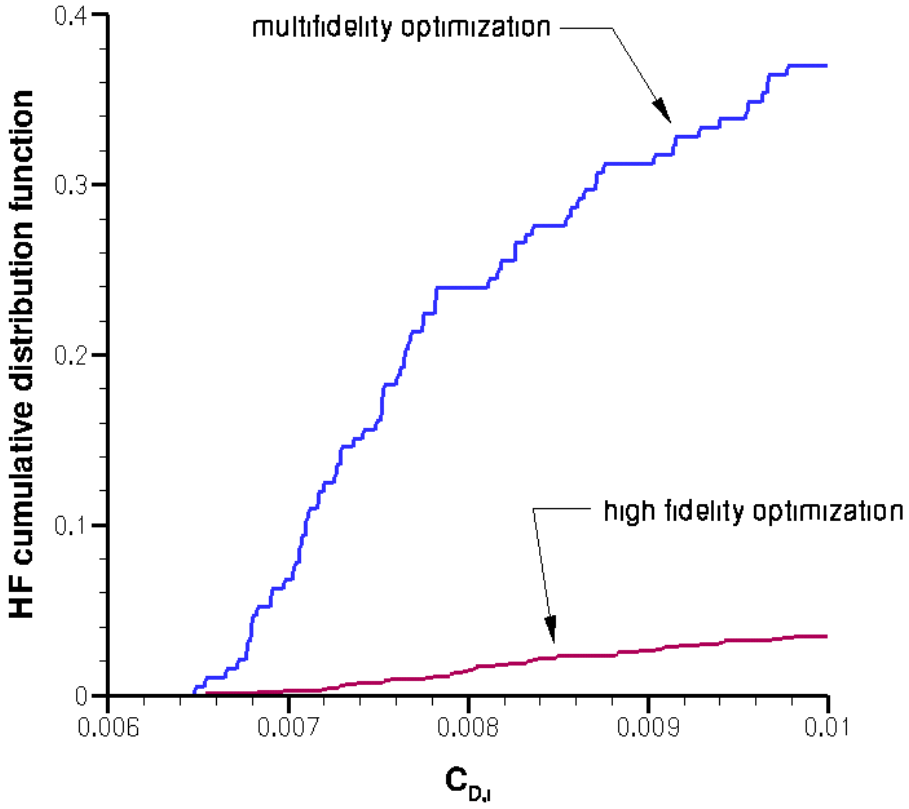

Figure 13. Quantification of multifidelity *vs.* high-fidelity-only optimization performance via aggregated cumulative distribution functions. The primary objective, $C_{D,i}$ is shown on the horizontal axis. The vertical axis is the numerically computed probability of finding feasible high-fidelity solutions exceeding the target on the x axis.

Statistical Results

It is important to realize that, due to the inherent coupling between the optimization path and the sequential radial basis function metamodel being created at the various stages of the optimization, the results depend on the initial conditions of the optimization (this is true whether using multifidelity or single fidelity optimization). **Figure 12**, for example, presents a different data profile for the same nominal problem as **Figure 11**, the only difference being the initial conditions.

For this reason, when comparing performance metrics, it is particularly important to expand results such as **Figures 11** and **12** and to consider ensembles in a statistical sense in order to draw meaningful conclusions. Thus, using multiple realizations with random initial conditions based on a Latin Hypercube design of experiments, optimization results were aggregated and analyzed as a group. When comparing multifidelity vs. high-fidelity-only optimization, care must also be exercised so that the exact same design variables are used in the initial design.

The details of this aggregate analysis are as follows. The candidate designs harvested as a result of each optimization are first filtered so that only the high-fidelity (HF) solutions that do not violate the constraints are considered.[13] These HF nonviolators are then sorted based on the primary objective (low $C_{D,i}$ in the present case). Aggregate performance profiles collected in this manner can then be analyzed in terms of the induced drag cumulative distribution function (CDF) of the wing designs. The example shown in **Figure 13** corresponds to 8 realizations of the three-dimensional optimization (**Table 7** subcase 3). The stopping criterion was based either on failure to improve the EI function (Eq. **(11)**), or reaching an imposed practical maximum of 24 high-fidelity solutions. The optimal designs for this case are given in the table below:

Method	$\alpha_0\ (^o)$	$d\alpha/dy\ (^o\, ft^{-1})$	$\theta_0\ (ft)$	C_L	$C_{D,i}$	$W_{wing}\ (lbs)$	σ_{VM}
MFSRBO	6.624	-0.704	0.0392	0.4624	6.484 x 10^{-3}	18.87	0.442
HF-only	6.418	-0.603	0.0384	0.4643	6.542 x 10^{-3}	18.64	0.471

Figure 13 shows that, by using multifidelity optimization, there is, for example, a 37% probability of achieving a drag coefficient less than 0.01, versus less than 4% with high-fidelity optimization only. Thus, for a given computational budget, there is an order of magnitude greater probability of finding/approaching the high-fidelity optimum by using multifidelity optimization.[14]

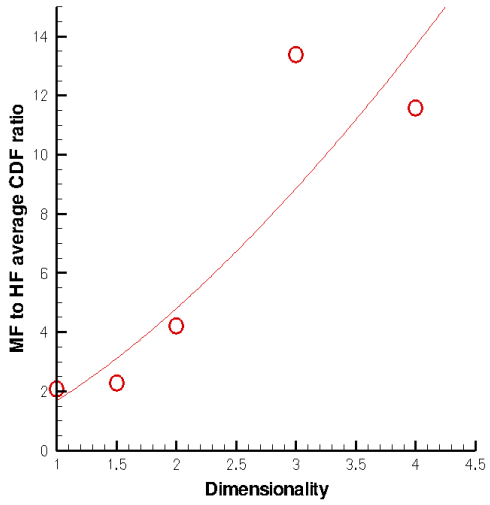

Figure 14. Relative efficiency between multifidelity and high-fidelity-only optimization as a function of design space dimensionality.

Neglecting, for the sake of simplicity, the cost of the low-fidelity analyses and the cost of the optimization calculations *per se*, the average ratio of the cumulative distribution functions provides an indication of the relative performance of these methods. Let us define the CDF area ratio as the ratio between the areas under the CDF curves (**Figure 13**) for $C_{D,i} \le 0.01$.

Figure 14 shows the CDF area ratio as a function of the search space dimensionality of the problem. The three- and four-dimensional cases are believed to be more typical of the expected performance ratio. Our observations suggest that the replicate-deterrent term **(13)**, may have had an important effect in the lower dimensional experiments, due to the effectively higher point density in those cases. The one-dimensional case was obtained by varying α_0 only. (The so-called 1.5-dimensional case represents a case where the constraints were such that only a narrow sliver of feasible solutions existed in the 2-D space, thus making the space effectively quasi-one-dimensional). While limited in scope and strictly empirical, the results of **Figure 14** suggest the possibility that the MFSRBO method may be increasingly beneficial as the dimensionality of the problem increases, although this question will be left for future research.

13 In this study, this was typically repeated for 8 to 16 realizations.

14 This is consistent with the prior MFSKO experience of the OSU members of our Team, which suggests dramatic benefits when the cost differential is high and the systematic errors are small.

5.2.3.2 UAV wing design

The baseline problem described above was extended to the case of an aeroelastic swept (UAV-type) wing at $M_\infty = 0.2$. The wing planform is a modified version of the European *SACCON* stability and control vehicle[15] with identical span and wing area. As in **Table 7** subcase 2 above, the design variables are the twist distribution, characterized by α_0 and $d\alpha/ds$. However, this time, the design objective is to maximize the pitch stability $-dC_m/d\alpha$, subject to minimum lift, maximum stress, and angular trim constraints as follows:

$$\begin{aligned} &\underset{\{\alpha_0,\, d\alpha/dy\}}{\text{minimize}} && dC_m/d\alpha \\ &\text{subject to} && C_L \geq (W_{payload}+W_{wing})/(q_\infty S_{ref}) \\ & && \sigma_{VM}/\sigma_{VM,max} < 0.55 \\ & && |C_m| < 0.002 \end{aligned} \qquad \textbf{(32)}$$

where C_m is the pitching moment about the root half chord location.

An example comparison of low- and high-fidelity results obtained using OPTMIS is shown in **Figure 15**,[16] corresponding to $\alpha_0 = 18.5^o$, $d\alpha/dy = -4.3^o\ ft^{-1}$ and $W_{payload} = 75\ lbs$ for an isotropic material with self-similar cross-section (see Section 4.4) and a spanwise-uniform maximum thickness of $\theta_0 = 0.025\ ft$.

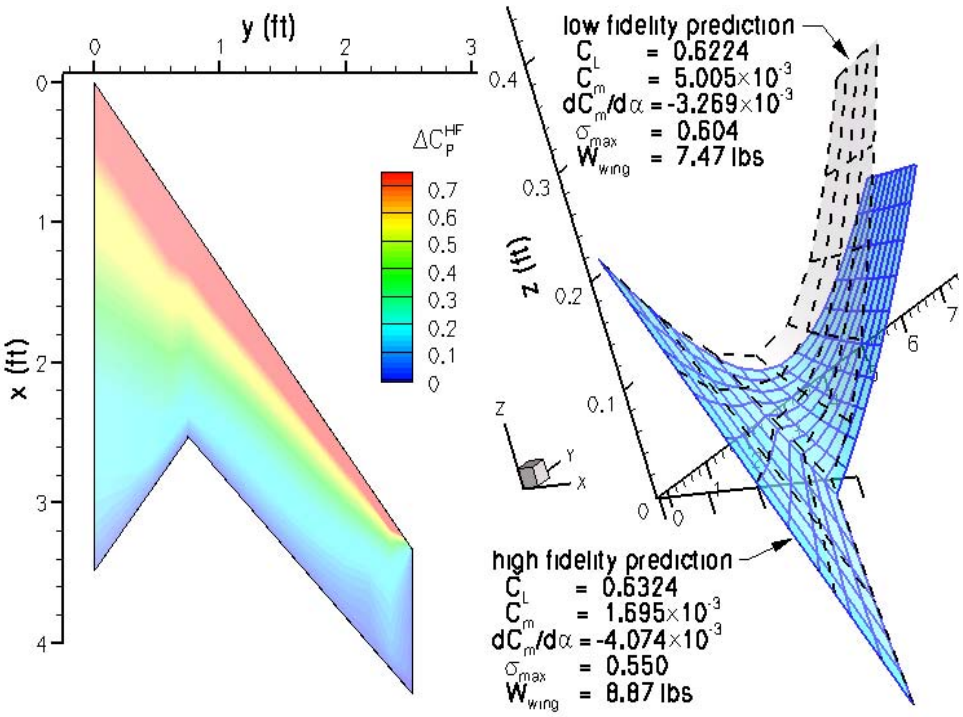

Figure 15. Low- and high-fidelity static aeroelastic deformation of UAV wing. (Left: planform view of loading. Right: perspective view of wing twist and bending (not to scale)).

The optimization methods and postprocessing metrics were identical to those used in Section 5.2.3.1. **Figure 16** provides an illustration of the multifidelity sequential radial basis optimization search path for a

15 NATO RTO, AVT-161 Assessment of Stability and Control Prediction Methods for NATO Air & Sea Vehicles.

16 "σ" in Figure 15 denotes the ratio $\sigma_{VM}/\sigma_{VM,max}$

given instance of a Latin Hypercube design of experiments including one high-fidelity and three low-fidelity solutions as the initial conditions. The flooded contours represent the primary objective, $dC_m/d\alpha$, which is noisy, due in part to finite differencing and to C_m being itself a sensitive quantity. As before, the large symbols denote high-fidelity analyses, while small symbols are used for low fidelity. Each symbol is colored based on the objective function, which is the stability derivative $dC_m/d\alpha$, augmented with penalty functions for violating either the lift, trim, or stress constraints. Specifically, the constraints are incorporated in the objective function using the following penalty formulation (using the previous values for W_{payload}, q_∞, and $S_{ref} = 4.15\,ft^2$):

$$
\begin{aligned}
f \;=\; & \frac{dC_m}{d\alpha} + 10.\max\left[|C_m| - 0.002\,,\,0\right] \\
& + 10.\max\left[\left(\frac{75 + W_{wing}}{40.76 \times 4.15}\right) - C_L\,,\,0\right] \\
& + 20.\max\left[\frac{\sigma_{VM}}{\sigma_{VM,\,max}} - 0.5\,,\,0\right]
\end{aligned}
\qquad \textbf{(33)}
$$

where W_{wing} is the structural weight of the wing, expressed in pounds.

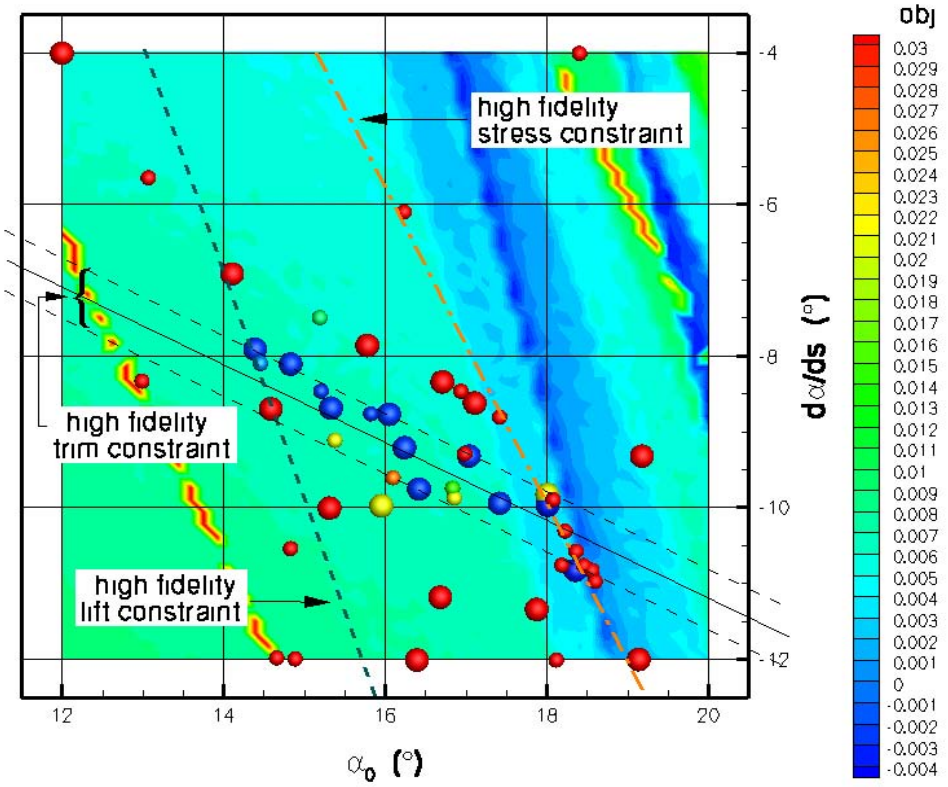

Figure 16. Sample multifidelity search path for UAV aeroelastic wing design problem.

Finally, **Figure 17** compares the aggregate cumulative distribution functions for the multifidelity and single fidelity optimizations, each based on eight random realizations. The resulting CDF area ratio, defined as the ratio between the areas under the CDF curves (**Figure 17**) for $dC_m/d\alpha \le -0.0027$, suggests 4:1 odds in favor of multifidelity optimization, versus high-fidelity only optimization.

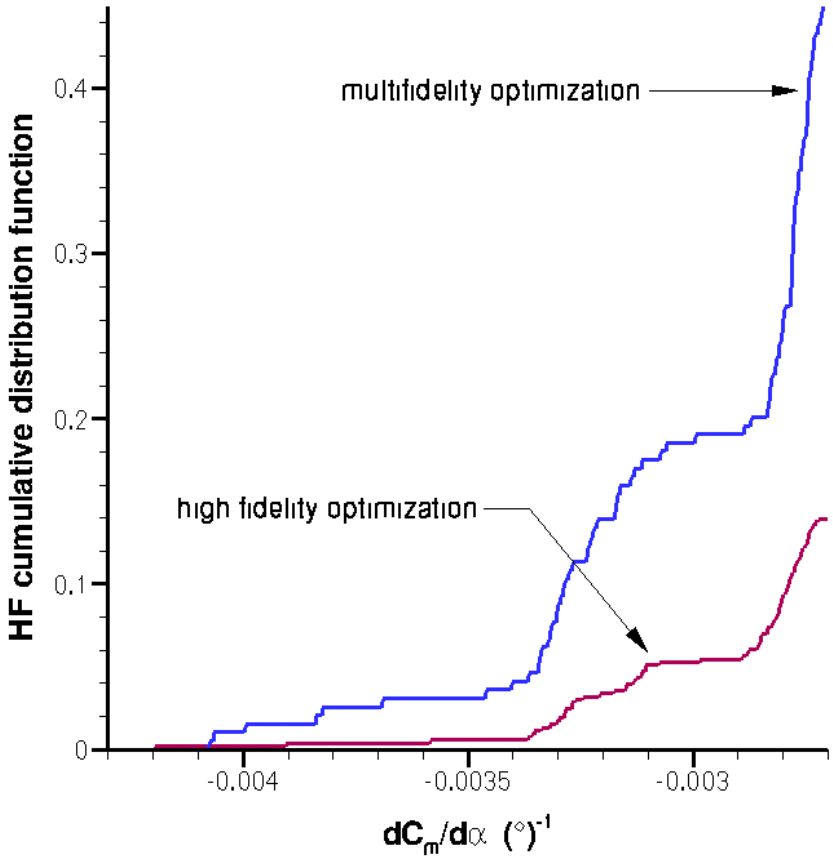

Figure 17. Quantification of multifidelity *vs.* high-fidelity-only optimization performance via aggregated cumulative distribution functions. The primary objective, $dC_m/d\alpha$ is shown on the horizontal axis. The vertical axis is the numerically computed probability of finding feasible high-fidelity solutions exceeding the target on the x axis.

6. DISCUSSION

This report has explored the use of radial basis functions instead of Kriging models in sequential multifidelity optimization. In adapting the methods, we have addressed at least three types of unavoidable challenges relating prediction, error estimation, and the expected improvement function. This investigation explored proposing two types of metamodeling approaches which are cascading (the most direct extension of Kriging-based methods with convergent prediction) and augmented dimensionality (which offers advantages for data starved cases).

Perhaps the greatest challenge was developing a comprehensive estimate of uncertainty corresponding to the approximate Bayesian intervals for Kriging functions. They are approximate because they are based on parameter estimates. Here, four types of approaches were considered with numerical results based on assumed errors and simple cross-validation. Finally, two alternative formulations for the expected improvement function were described because of the computational challenge of estimating correlation for the radial basis function case.

7. CONCLUSIONS AND FUTURE WORK

The preliminary numerical results indicate that methods based on radial basis functions can compete with Kriging methods in relation to efficiently and repeatedly identifying global optimal solutions. As a result, the radial basis functions might seem to be preferred for the following reasons:

- **Reduced computational overhead** – Radial basis function estimation does not require likelihood minimization since we have a closed form for the coefficient estimates. Thorough and accurate likelihood optimization is a difficult computational challenge. The efficiency increase through eliminating one of the two optimizations per iteration (the other is expected improvement optimization) can enable many new applications of related methods. These included so-called "on-line" or automatic optimal decision-making. For example, data can stream in from sensors or simulations running in parallel and be quickly integrated for determining optimal settings and requests for additional inputs.
- **Improved numerical stability** – In the prior computational work of the OSU members of our Team, generated by Huang, Allen, Notz, and Miller (2006), we encountered several crashes from numerical inversions in deriving numerical results. These problems likely were not fully understood by us. However, our preliminary conclusion was that the errors occurred because of the spacing off design points near each other and on a lattice and could not be avoided through the use of singular value decomposition-based inversion. By contrast, the radial basis function fitting is based on linear model estimation which is very stable using singular value decomposition (Press, Teukolsky, Vetterling, and Flannery, 2007).
- **No stationarity assumption** – In the Huang, Allen, Notz, and Miller method there was a check for violation of the assumption that systematic errors have zero expected mean. The methods included a potentially expensive checking and adjustment process which was not fully reflected in the measured computational performance. The methods based on radial basis functions seem to require no comparable steps which could offer computational advantages.

Table 11 qualitatively compares alternative methods in relation to modeling approach, computational overhead, available convergence results, and test performance. The tentative conclusion is that further hybrid methods based on radial basis functions are a promising topic for research. The developed methods will likely offer reduced modeling overhead, theoretical convergence results, and good test performance on numerical examples and real-world problems.

Table 11. Overview of alternative methods. *Developed in this project.. **Proposed for future development.

Method	Modeling	Modeling Overhead	Convergence	Test Performance
SKO (Jones et al. & Huang, et al. #1)	Kriging	Likelihood Optimization	Not-established	Generally Global
SRBO*	RBF	LSE	Not-established	Competitive
MFSKO (Huang. Allen et al. #2)	Kriging	Likelihood Optimization	Not-established	Generally Global
Trust Region (Rodriguez, Renaud,…)	Polynomial	LSE	Established	Not Competitive
MFSRBO: Assumed Variance*	RBF	LSE	Not-established	Competitive
MFSRBO: Cascading model*	RBF	LSE	Not-established	Not studied
MFSRBO: PRESS*	RBF	PRESS Cross Validation	Not-established	Not studied
Simple Hybrid*	RBF	LSE	Established	Not Competitive
Hypothetical Future Hybrid Method**	RBF	LSE	Promising	Competitive

The research has also uncovered many remaining challenges. These include:

- **Developing globally convergent, efficient, hybrid methods** – The simple hybrid methods considered always converge to local minima and might likely converge to global minima under the assumptions considered. Yet, their computational performance has not been studied and is likely not competitive. Also, the assumptions of deterministic responses and continuously adjustable fidelity levels might need to be relaxed. It is possible that new classes of hybrid methods will offer competitive computational performance and proven convergence.

- **Error estimation including bias** – The errors used in the proposed MFSRBO explored in our computational studies are based on regression variance errors only. This makes their interpretation difficult in deterministic cases, i.e., cases with perfect repeatability error or $\sigma = 0$. In such cases, the intervals do not directly correspond to any interpretable physical quantity in the corresponding problem and performance of the methods likely is degraded. Developing new methods based on measures of bias such as regression C_p or diagnostics proposed in Tseng (2007) is a promising avenue of research.
- **Measuring computational overhead** – It is clear that linear model estimation is computationally superior to likelihood estimation in Kriging models. Yet, so far we have not measured the computational advantages. Also, we have not tuned the methods to the point at which the overhead is minimal and comparable to standard nonlinear programming methods. The promising results from the radial basis function methods here suggest that such performance is achievable.
- **More thorough computational comparisons** – There are several cases in which further comparisons can shed light on the conditions under which radial basis function methods are competitive or superior to methods based on Kriging models and/or trust region methods. Further comparisons are possible, particularly including discrete or categorical factors.
- **Parallelizing the methods** – One promising area that we considered was the possibility to parallelize function evaluations. For example, it is advantageous to launch one slow, high-fidelity simulation simultaneous with several low-fidelity simulations. The structure of related methods lends itself nicely to parallel processing with its significant computational advantages.

REFERENCES

Alexandrov, N. M., Dennis, J. E., Jr., Lewis, R. M., and Torczon, V., "A Trust Region Framework for Managing the Use of Approximation Models in Optimization," *Structural Optimization*, Vol. 15, No. 1, 1998, pp. 16-23.

Alexandrov, N. M., Lewis, R. M., Gumbert, C. R., Green, L. L., and Newman, P. A., "Optimization with Variable-Fidelity Models Applied to Wing Design," AIAA-2000-0841, Jan. 2000.

Allen, T. T., *Introduction to Discrete Event Simulation Theory with Applications: Voting Systems, Health Care, Military, and Manufacturing*, Springer Verlag, 2010.

Allen, T. T., *Introduction to Engineering Statistics and Lean Sigma: Statistical Quality Control and Design of Experiments and Systems*, 2nd ed., Springer Verlag, 2010.

Antanas, Z., "On similarities between two models of global optimization: statistical models and radial basis functions," *Journal of Global Optimization*, published online, DOI 10.1007/s10898-009-9517-9, 2010.

Beran, P. S., Lindsley, N. J., Camberos, J., and Kurdi, M., "Stochastic Nonlinear Aeroelasticity," AFRL-RB-WP-TR-2009-3057, Jan. 2009.

Björkman M., Holmström K., "Global optimization of costly nonconvex functions using radial basis functions," *Optim. Eng*. Vol. 1, No, 4, 2010, pp. 373–397.

Branin, F. H. "Widely Convergent Methods for Finding Multiple Solutions of Simultaneous Nonlinear Equations," *IBM Journal of Research Developments*, 16, 1972, pp. 504-522.

Chang, K. J., Haftka, R. T., Giles, G. L., and Koa, P.-J., "Sensitivity-Based Scaling for Approximating Structural Response," *J. Aircraft*, Vol. 30, No. 2, Mar.-Apr. 1993, pp. 283-288.

Dillenius, M. F. E., Lesieutre, D. J., Hegedus, M. C., Perkins, S. C., Jr., Love, J. F., and Lesieutre, T. O., "Engineering-, Intermediate-, and High-Level Aerodynamic Prediction Methods and Applications," *Journal of Spacecraft and Rockets*, Vol. 36, No. 5, Sep.-Oct. 1999, pp. 609-620.

Dufresne, S., Johnson, C., and Mavris, D. N., "Variable Fidelity Conceptual Design Environment for Revolutionary Unmanned Aerial Vehicles," *J. Aircraft*, Vol. 45, No. 4, Jul.-Aug. 2008, pp. 1405-1417.

DuMouchel, W. and Jones, B., "A Simple Bayesian Modification of D-optimal Designs to Reduce Dependence on an Assumed Model". *Technometrics* 36, 1994, pp. 37-47.

Eldred, M. S., Giunta, A. A., and Collis, S. S., "Second-Order Corrections for Surrogate-Based Optimization with Model Hierarchies," AIAA 2004-4457, Aug. 2004.

Floudas, C. A. and Gounaris, C. E., "A Review of Recent Advances in Global Optimization," *Journal of Global Optimization*, Vol. 45, 2009, pp. 3-38.

Forrester, A. I. J. and Keane, A. J., "Recent Advances in Surrogate-Based Optimization," *Prog. Aero. Sci.*, Vol. 45, Issues 1-3, Jan.-Apr. 2009, pp. 50-79.

Gablonsky, J. M. and Kelley, C. T., "A Locally-biased Form of the Direct Algorithm, *Journal of Global Optimization*, Vol. 21, 2001, pp. 27-37.

Gardner, D. R. and Hennigan, G. L., "On Developing a Multifidelity Modeling Algorithm for System-Level Engineering Analysis," SAND 2003-0399, Feb. 2003.

Ghoreyshi, M., Badcock, K. J., and Woodgate, M. A., "Integration of Multi-Fidelity Methods for Generating an Aerodynamic Model for Flight Simulation," AIAA 2008-197, Jan. 2008.

Gutmann, H.-M., "A Radial Basis Function Method for Global Optimization, *Journal of Global Optimization*, Vol. 19, 2001, pp. 201-227.

Hatanaka, K., Obayashi, S., and Jeong, S., "Application of the Variable-Fidelity MDO Tools to a Jet Aircraft Design," Presented at the 25th International Congress of the Aeronautical Sciences, Hamburg, Germany, Sep. 3.-8, 2006.

Holden, C. M. E. and Keane, A. J., "Visualization Methodologies in Aircraft Design," AIAA 2004-4449, Sep. 2004.

Holmström, K (2008), An Adaptive Radial Basis Algorithm (ARBF) for Expensive Black-box Global Optimization, *Journal of Global Optimization*, Vol. 41, No.3, pp. 447-464.

Hutchinson, M. G., Unger, E. R., Mason, W. H., Grossman, B., and Haftka, R. T., "Variable-Complexity Aerodynamic Optimization of a High Speed Civil Transport Wing," *J. Aircraft*, Vol. 31, 1994, pp. 110-116.

Huang, D. and Allen, T., "Design and Analysis of Variable Fidelity Experimentation Applied to Engine Valve Heat Treatment Process Design," *J. Royal Statistical Soc.: Series C*, Vol. 54, 2005, pp. 1-21.

Huang, D., Allen, T. T., Notz, W. I., and Miller, R. A., "Sequential Kriging Optimization Using Multiple Fidelity Evaluations," *Structural and Multidisciplinary Optimization*, Vol. 32, No. 5, Nov. 2006, pp. 369-382.

Huang, D., Allen, T. T., Notz, W. I., and Zheng, N., "Global Optimization of Stochastic Black-Box Systems via Sequential Kriging Meta-Models," *J. Global Opt.*, Vol. 34, No. 3, Mar. 2006, pp. 441-466.

Humphrey, D.G. and Wilson, J.R., "A Revised Simplex Search Procedure for Stochastic Simulation Response-Surface Optimization," *INFORMS Journal on Computing*, Vol. 12, 2000, pp. 272-283.

Jakobsson S., Patriksson M., Rudholm, J., and Wojciechowski, A., "A Method for Simulation Based Optimization using Radial Basis Function," *Optimization and Engineering*, online published, 10.1007/s11081-009-9087, 2009.

Jarrett, J. P., "Multi-Fidelity Gradient-Based Optimization in Turbomachinery Aerodynamic Design," AIAA 2006-1907, May 2006.

Jones, D., Schonlau, M. and Welch, W., "Efficient Global Optimization of Expensive Black-Box Functions,"*Journal of Global Optimization*," Vol.13, pp. 455-492.

Jyotsula, U., Sudhakar, K., Mujumdar, P. M., and Isaacs, A., "Fidelity Uncertainty Characterization Leading to Robust Design," SAROD-2005.

Kaufman, M., Balabanov, V., Burgee, S. L., Giunta, A. A., Grossman, B., Mason, W. H., and Watson, L. T., "Variable Complexity Response Surface Approximations for Wing Structural Weight in HSCT Design," AIAA-96-0089, Jan. 1996.

Keane, A. J., "Wing Optimization Using Design of Experiment, Response Surface, and Data Fusion Methods," *J. Aircraft*, Vol. 40, No. 4, 2003, pp. 741-750.

Kennedy, M. C. and O'Hagan, A., "Predicting the Output of a Complex Computer Code When Fast Approximation are Available," *Biometrika*, Vol. 87, No. 1, 2000, 1-13.

Laguna, M., Molina, J., Perez, F., Caballero, R., Hernandez-Diaz, A G., "The Challenge of Optimizing Expensive Black Boxes: A Scatter Search/Rough Set Theory Approach," *Journal of the Operational Research Society*, Vol. 61, 2010, pp. 53-67.

Leary, S. J., Bhaskar, T., and Keane, A. J., "A Knowledge-Based Approach To Response Surface Modelling in Multifidelity Optimization," *Journal of Global Optimization*, Vol. 26, 2003, pp. 297-319.

Lesieutre, D. J., Lesieutre, T. O., and Dillenius, M. F. E., "Planform/Configuration Optimization Program OPTMIS for Arbitrary Cross Section Configurations With Up To Two Fin Sets - Software User's Manual and Software Programmer's Manual," NEAR TR 519, Nielsen Engineering & Research, Apr. 1997.

Lesieutre, D. J., Lesieutre, T. O., and Dillenius, M. F. E., "Optimal Aerodynamic Design of Advanced Missile Configurations With Geometric and Structural Constraints," NEAR TR 520, Nielsen Engineering & Research, Sep. 1997.

Lesieutre, D. J., Dillenius, M. F. E., and Lesieutre, T. O., "Multidisciplinary Design Optimization of Missile Configurations and Fin Planforms for Improved Performance," 7th Symposium on Multidisciplinary Analysis and Optimization, St. Louis, MO, Sep. 1998.

Lewis, K. and Mistree, F., "The Other Side of Multidisciplinary Design Optimization: Accommodating a Multiobjective, Uncertain and Non-Deterministic World," *Eng. Opt.*, Vol. 31, 1998, pp. 161-189.

Madsen, J. I. and Langthjem, M., "Multifidelity Response Surface Approximations for the Optimum Design of Diffuser Flows," *Optimization and Engineering*, Vol. 2, 2001, pp. 453-468.

Press, W., Teukolsky, S., Vetterling, W. and Flannery, B., "*Numerical Recipes: The Art of Scientific Computing*," Third Edition, Cambridge University Press, 2007.

Queipo, N. V., Haftka, R. T., Shyy, W., Goel, T., Vaidyanathan, R., and Tucker, P. K., "Surrogate-Based Analysis and Optimization," *Prog. Aero. Sci.*, Vol. 41, 2005, pp. 1-28.

Regis, R. G .and Shoemaker, C. A. "Improved Strategies for Radial Basis Function Methods for Global Optimization,"*Journal of Global Optimization*, Vol. 37, pp. 113-135.

Reisenthel, P. H., Love, J. F., Lesieutre, D. J., and Dillenius, M. F. E., "Innovative Fusion of Experiment and Analysis for Missile Design and Flight Simulation," *NATO-RTO Symposium on Innovative Missile Systems,* RTO-MP-AVT-135, Amsterdam, The Netherlands, May 2006.

Reisenthel, P. H., Love, J. F., Lesieutre, D. J., and Childs, R. E., "Cumulative Global Metamodels With Uncertainty -- A Tool for Aerospace Integration," *The Aeronautical Journal*, June 2006, pp. 375-384.

Reisenthel, P. H., Childs, R. E, and Higgins, J. E., "Surrogate-Based Design Optimization of a Large Asymmetric Launch Vehicle Payload Fairing," AIAA 2007-361, Jan. 2007.

Reisenthel, P. H. and Lesieutre, D. J., "Cumulative Metamodeling With Uncertainty Estimation: A New Approach to Risk-Based Optimization of Aerospace Vehicles," NEAR TR 632, Nielsen Engineering & Research, Mountain View, CA, Jul. 2007.

Robinson, T. D., Eldred, M. S., Willcox, K. E., and Haimes, R., "Strategies for Multifidelity Optimization with Variable Dimensional Hierarchical Models," AIAA 2006-1819, May 2006.

Robinson, T. D., Willcox, K. E., Eldred, M. S., and Haimes, R., "Multifidelity Optimization for Variable-Complexity Design," AIAA 2006-7114, Sep. 2006.

Rodriguez, J. F., Renaud, J. E., and Watson, L. T., "Convergence of Trust Region Augmented Lagrangian Methods using Variable Fidelity Approximation Data," *Structural Optimization*, Vol. 15, pp. 141-156.

Rodriguez, J. F., Perez, V. M., Padmanabhan, D., and Renaud, J. E., "Sequential Approximate Optimization Using Multiple Fidelity Response Surface Approximation," *Structural and Multidisciplinary Optimization*, Vol. 22, No. 1, 2001, pp. 23-34.

Sacks, J., Schiller, S. B., and Welch, W., "Design for Computer Experiments," *Technometrics*, Vol. 31, 1989, pp. 41-47.

Schenk, J. R., Huang, D., Zheng, N., and Allen, T. T., "Multiple Fidelity Simulation Optimization of Hospital Performance Under High Consequence Event Scenarios," Proceedings of the 37th Winter Simulation Conference, edited by M. E. Kuhl, N. M. Steiger, F. B. Armstrong, and J. A. Joines, 2005.

Spall, J.C., "Implementation of the Simultaneous Perturbation Algorithm for Stochastic Optimization," *IEEE Transactions on Aerospace and Electronics Systems*, Vol. 34, 817-823.

Singh, G. and Grandhi, R. V., "Mixed-Variable Optimization Strategy Employing Multifidelity Simulation and Surrogate Models," *AIAA Journal*, Vol. 48, No. 1, 2010.

Schonlau, M., *Computer Experiments and Global Optimization*, Ph.D. Dissertation, University of Waterloo, 1997.

Sóbester, A., Leary, S. J., and Keane, A. J., "On the Design of Optimization Strategies Based on Global Response Surface Approximation Models, *J. Global Opt.*, Vol. 33, No. 1, 2005, pp. 31-59.

Sun, J., Zhang, G., Vlahopoulos, N., and Hong, S.-B., "Multi-Disciplinary Design Optimization under Uncertainty for Thermal Protection System Applications," AIAA 2006-7002, Sep. 2006.

Swiler, L. P., "Bayesian Methods in Engineering Design Problems," SAND2005-3295, Sandia National Laboratories, Apr. 2006.

Tseng, S.H., "Bayesian and Semi-Bayesian Regression Applied to Manufacturing Wood Products," Ph.D. Dissertation at The Ohio State University, 2007.

Villemonteix, J., Vazquez, E., Walter, E., "An Informational Approach to the Global Optimization of Expensive-to-Evaluate Functions," *Journal of Global Optimization*, Vol. 44, pp. 509-534.

Wintzer, M., Sturdza, P., and Kroo, I., "Conceptual Design of Conventional and Oblique Wing Configurations for Small Supersonic Aircraft," AIAA 2006-930, Jan. 2006.

LIST OF ABBREVIATIONS / ACRONYMS / SYMBOLS

AFRL	Air Force Research Laboratory
AR	Aspect Ratio (total span over chord)
arg	Argument
c	Chord length
C	Cost
$C_{D,i}$	Induced drag coeffient
CDF	Cumulative Distribution Function
CDL	Cross-Disciplinary Link
CFD	Computational Fluid Dynamics
C_L	Lift coefficient
C_m	Pitching moment coefficient
CSD	Computational Structural Dynamics
CSM	Computational Structural Mechanics
d	Design space dimensionality
DIRECT	Optimization method developed by Gablonsky et al. (2001)
DOE	Design of Experiments

EGO	Efficient Global Optimization
EI	Expected Improvement
f	Function
$\vec{F}_i$	Force vector
FEM	Finite Element Method
g	Constraint
GCV	Generalized Cross Validation
HF	High-Fidelity
KKT	Karush-Kuhn-Tucker
KRG	Kriging-based regression
LER	Leading Edge Radius
LF	Low-Fidelity
LSE	Least Squares Estimation
MAV	Micro Air Vehicle
max	Maximum
MDA	Multidisciplinary Design Analysis
MDA	Multidisciplinary Design Optimization
MFSKO	Multifidelity Sequential Kriging Optimization
MFSRBO	Multifidelity Sequential Radial Basis Optimization
min	Minimum
MLS	Moving Least Squares
N[μ,σ]	Random process with normal distribution of mean μ and standard error σ
NEAR	Nielsen Engineering & Research
obj	Objective function
OSU	Ohio State University
P[ ]	Probability
Param.	Parametric
PRESS	Prediction Error Sum of Squares
PRG	Polynomial regression
qParam.	Quasi parametric
q_∞	Freestream dynamic pressure
RBF	Radial Basis Function
ref	Reference quantify
RS	Response Surface
RSS	Revised Simplex Search
S	Area
s(f)	Standard error of function f
SKO	Sequential Kriging
SPSA	Simultaneous Perturbation Stochastic Approximation
SRBO	Sequential Radial Basis Optimization
STTR	Small Business Technology Transfer
SVD	Singular Value Decomposition
SVR	Support Vector Regression
TH	Maximum structural thickness at a given span location
$\vec{u}_i$	Velocity vector
UAV	Unmanned Aerial Vehicle
Var	Variance
W	Weight
x	Streamwise coordinate
$\mathbf{x}$	Design vector
$\mathbf{X}$	Design matrix

y	Spanwise coordinate
$\mathbf{Y}$	Dependent variables data vector
z	Normal coordinate
$\hat{}$	Estimated value
$*$	Effective best solution
α	Angle of attack
α_o	Root chord angle of attack
γ	Metamodel parameter
$\vec{\Gamma}_i$	Circulation
ΔC_p	Differential pressure coefficient
Λ	Taper ratio
ρ	Fluid density
σ_{VM}	Von Mises stress
θ_o	Root chord maximum structural thickness

APPENDIX A – CORRELATION COEFFICIENT COMPUTATION

The objective function of the optimization is the multifidelity expected improvement function driver EI(**x**,*l*) (see Eq. (11)). At any given point **x** within the optimization search, the fidelity-maximization of EI(**x**,*l*) results primarily from the balance between the cost ratio $\alpha_3(l)$ and the local correlation $\alpha_1(\boldsymbol{x},l)$ between fidelity levels *l* and *m*, i.e., $\alpha_1(\boldsymbol{x},l) = \mathrm{corr}\left[\hat{f}_l(\boldsymbol{x}), \hat{f}_m(\boldsymbol{x})\right]$. This term is key to the functioning of the method: whenever lower and higher fidelity estimates are correlated, the optimization favors the lower cost function, and where they are sufficiently uncorrelated,[17] the high-fidelity estimate takes priority.

In the augmented dimensionality version of our method, the correlation coefficient $\alpha_1(\boldsymbol{x},l)$ is computed numerically as the correlation coefficient between two data streams. The two data streams consist of local sets $\left\{f_l(\boldsymbol{x}_0),\ldots,f_l(\boldsymbol{x}_q)\right\}$ and $\left\{f_m(\boldsymbol{x}_0),\ldots,f_m(\boldsymbol{x}_q)\right\}$, where $\left\{\boldsymbol{x}_0,\ldots,\boldsymbol{x}_q\right\}$ denotes a set of points in the immediate neighborhood of **x**, and f is the metamodel response. In practice, one must decide on what these neighbor points should be (scale of coverage, spatial pattern, and number).

Our implementation "piggy backs" on the search stencil of the steepest ascent, hill climbing algorithm used in NEAR RS (Section 4.3.6). In its simplest form (but not the most efficient), the stencil consists of a center point ($\boldsymbol{x}_0 = \boldsymbol{x}$) and the vertices of a hypercube of size ***L***, centered on **x**. In our search strategy, ***L*** is initiated at some user-prescribed initial value around the random seed points.[18] The stencil is then interrogated at each of the vertices. If an improvement is possible the search location is moved to the vertex corresponding to the *best* improvement (steepest ascent), leaving ***L*** unchanged. If, on the other hand, there is no improvement at any of the vertices, then the pattern remains centered on x_0 and ***L*** is cut in half. The algorithm goes on until reaching a maximum user-prescribed number of recursion levels (effectively defining the maximum resolution of our search).

For the purposes of computing the correlation coefficient, the local length scale ***L*** is a natural choice for defining the scale of coverage of the neighborhood set $\left\{\boldsymbol{x}_0,\ldots,\boldsymbol{x}_q\right\}$. In this study, a *d*-dimensional hypercube of size ***L/2*** with *w* = 3 points per side was used for most of the cases, providing reasonably smooth estimates of the correlation coefficient.

17 (for a given cost ratio)

18 The random seed points are the initializations of the multistart method.

APPENDIX B – CONVERGENCE CONDITIONS

Trust region augmented Lagrangian multifidelity methods have been proven to converge to local optima of the highest fidelity system (Rodriguez, Renaud, and Watson, 1998). Yet, their assumptions include that the systems are deterministic and that the fidelity level, ψ, can be continuously adjusted. In the context of multiple local minima they can be considered inferior since sequential optimization methods using global metamodels have been demonstrated on test problems to converge efficiently to the global optimum.

The purpose of this system is to clarify the conditions used to prove the trust region convergence. As a result, reviewing the assumptions from Rodriguez, Renaud, and Watson (1998) clarifies the convergence criteria for hybrid methods. It also illuminates the conditions and issues for future, more efficient hybrid optimization method convergence. The notation was somewhat different than in proceeding sections. The relationship is clarified below.

k	Lagrangian iteration
s	approximate minimization iteration
i, j, l	variable indices
m	number of inequality constraints
n	number of design variables
p	number of equality constraints
$f(\mathbf{x})$	objective function
$g(\mathbf{x})$	inequality constraint vector
$g_j(\mathbf{x})$	j-th inequality constraint
$h(\mathbf{x})$	equality constraint vector
$h_i(\mathbf{x})$	i-th equality constraint
r_p	penalty parameter
$\mathbf{x}$	design vector, dimension n
x_l	l-th design variable
$\mathbf{x}^U$	upper bound vector, dimension n
x^U_l	l-th design upper bound
$\mathbf{x}^L$	lower bound vector, dimension n
x^L_l	l-th design lower bound
$\mathbf{B}$	approximation of the Hessian
K	constraints residual
S	design space
$\beta, \beta_1, \beta_2, k$	scalars
$\varepsilon_1, \varepsilon_2$	convergence tolerance
$\gamma_0, \gamma_1, \gamma_2, \eta, \mu$	trust region parameter
λ	Lagrange multiplier vector, dimension $m+p$
λ_i	i-th Lagrange multiplier
ρ	trust region ratio
ψ	fidelity control
$\|.\|$	Euclidean norm
∇	Gradient operator with respect to design vector x
$P[y(\mathbf{x})]$	Projection operator; projects the vector y onto the set of feasible directions at $\mathbf{x}$
Δ	trust region radius
$\Delta\mathbf{x}$	step size

Given minimization problems, authors made several assumptions as follow:

Min: $f(\mathbf{x})$ **(34)**
Subject to
$h_i(\mathbf{x}) = 0,\ i = 1, \ldots, p,$: equality const **(35)**
$g_j(\mathbf{x}) \geq 0, j = 1,\ldots,m,$: inequality const. **(36)**
$x^L{}_l < x_l \leq x^U{}_l,\ l = 1,\ldots,n.$: bounds **(37)**

which is equivalent to Eq. (10) using:

$$f_m(\mathbf{x},\lambda,r_p) = f(\mathbf{x}) + \Sigma_{i=1,\ldots,p}\,[\lambda_i h_i(\mathbf{x}) + r_p h_i(\mathbf{x})^2] + \Sigma_{j=1,\ldots,m}[\lambda_{p+j}\Psi_j(\mathbf{x}) + r_p \Psi_j(\mathbf{x})^2] \quad \textbf{(38)}$$

In terms of these definitions, the nine key assumptions are as follows. It is not clear whether all nine are really needed and they relate generally to bounds on the roughness of relevant functions. Notes follow each assumption. Overall, these assumptions might be considered relevant to many types of modeling problems that do not involve hits or misses of moving components or other forms of highly discontinuous physical behaviors.

AS1. Design space, *S,* has a nonempty interior and compact, i.e., it contains its boundary.

AS2. Objective function (f), inequality constraints (g_i), and equality constraints (h_i) are twice continuously differentiable on an open set containing the design space *S*.

AS3. The objective function (the augmented Lagrangian function), $\nabla f_l(\mathbf{x})$, satisfies a Lipschitz condition. In words, the gradients are bounded.

AS4. The feasible set defined by the inequality constraints, equality constraints, and upper and lower bounds is nonempty.

AS5. Trust region ratio, ρ^S, $\rightarrow 1$ as trust region radius, $\Delta^S \rightarrow 0$ or fidelity control, $\psi \rightarrow \psi_{max}$.
Trust region "ratio" is as follow by the authors, *s* is the iteration counter for the number of approximate augmented Lagrangian minimizations. If $\rho^S \leq 0$, the approximation is bad and the trust region radius, Δ^S should be reduced. If $\rho^S \geq 1$, the approximation is also bad but the direction is right. If $\rho^S \subset (0, 1)$, the radius can be kept unchanged, reduced, or increased based on how close to 0 or 1 it is.

$$\rho^S = \frac{\Phi\left(x^k,\lambda^k,r_p^k\right) - \Phi(x^{k,s},\lambda^k,r_p^k)}{\widetilde{\Phi}\left(x^k,\lambda^k,r_p^k\right) - \widetilde{\Phi}(x^{k,s},\lambda^k,r_p^k)}$$

AS6. Inequality constraint vector, **g** and equality constraint vector, **h** satisfy the Kuhn-Tucker constraint qualification or the modified Arrow-Hurwicz-Uzawa constraints qualification at any local minimum.

- KKT constraint qualification – i) ACQ(Abadie constraint qualification) – the tangent cone of a feasible set at a feasible point $\mathbf{x}^*$ is the linearized cone at $\mathbf{x}^*$ in the tangent cone, ii) LICQ(Linear independence constraint qualification) – the rows of Jacobian matrices for inequality and equality constraints are linearly independent (from a note of The Karush-Kuhn-Tucker Theorem, by Moritz Kuhn, 2006)

AS7. The Jacobian matrix of the active constraints has full rank at any limit point $\mathbf{x}^*$ of the sequence $\{\mathbf{x}^k\}$ considered.

AS8. The set $M \triangleq \{\{x|\Phi(x) < \Phi(x^0)\} \cap \{x^L \leq x \leq x^U\}\}$ with $\mathbf{x}^0$ satisfying $\mathbf{x}^L_i \leq \mathbf{x}_i \leq \mathbf{x}^U_i$ ($i = 1, \ldots, n$) is not empty.

- It is necessary that the solution of the optimization problem be nontrivial.

AS9. Approximation of Hessian, $\| \mathbf{B} \| \leq$ an assumed constant.

- It is necessary to assure that the Hessian (containing the second derivatives) approximation remains uniformly bounded.

APPENDIX C – DISCUSSION ON THE HANDLING OF CONSTRAINTS

The minimum induced drag design considered in the baseline problem of Section 5.2.3.1 exercised structural and aerodynamic constraints. Specifically, the following problem was solved:

$$\begin{aligned} &\underset{\{\alpha_0,\, d\alpha/dy,\, \theta_0,\, \Lambda\}}{\text{minimize}} && C_{D,i} \\ &\text{subject to} && C_L \geq (W_{payload} + W_{wing})/(q_\infty S_{ref}) \\ & && \sigma_{VM} / \sigma_{VM,max} < 0.5 \end{aligned} \tag{39}$$

The constraints were incorporated into the objective function using a simple penalty method, specifically ($W_{\text{payload}} = 75\ lbs$, $q_\infty = 40.76\ psf$ and $S_{ref} = 5\ ft^2$):

$$f \;=\; C_{D,i} + 10.\max\left[\left(\frac{75 + W_{wing}}{40.76 \times 5}\right) - C_L, 0\right] + 20.\max\left[\frac{\sigma_{VM}}{\sigma_{VM,max}} - 0.5, 0\right] \tag{40}$$

where W_{wing} is the structural weight of the wing, expressed in pounds. The process of maximizing the multifidelity expected improvement function **(11)** involves calculating **(15)**, which requires keeping track of the current best effective solution $\boldsymbol{x}^* = [\alpha_0^*, (d\alpha/dy)^*, \theta_0^*, \Lambda^*]$, and the ability to estimate the objective function f and its variance s^2 at any design point $\boldsymbol{x}$ for any level of fidelity.

Each independent metamodel surrogate for $C_{D,i}$, C_L , W_{wing} , and $\sigma_{VM}/\sigma_{VM,max}$ yields an estimated value (denoted with a $(\hat{})$) and standard error s . The approach used in this work considers the primary objective $C_{D,i}$ as probabilistic. However, for simplicity, the constraints were treated as deterministic. Thus

$$\hat{f} \;=\; \hat{C_{D,i}} + 10.\max\left[\left(\frac{75 + \hat{W_{wing}}}{40.76 \times 5}\right) - \hat{C_L}, 0\right] + 20.\max\left[\frac{\hat{\sigma_{VM}}}{\hat{\sigma_{VM,max}}} - 0.5, 0\right] \tag{41}$$

but

$$s(f) \;=\; s(C_{D,i}) + 0.s(C_L) + 0.s(W_{wing}) + 0.s\left(\frac{\sigma_{VM}}{\sigma_{VM,max}}\right) \tag{42}$$

A better, fully probabilistic, approach which takes into account the *probability* of constraint violation is described in Forrester et al. (2009), in which the expected improvement is replaced by the expectation of improving of the objective f while simultaneously being a feasible design:

$$E\left[\max\left(\hat{f}_m(\boldsymbol{x}^*) - \hat{f}_m(\boldsymbol{x}), 0\right) \cap \{g > g_{\min}\}\right] \tag{43}$$

In **(43)**, g represents a constraint and $g > g_{\min}$ represents the condition for feasible designs. In the case where primary objective and constraint are uncorrelated, the expectation **(43)** can be expressed as a simple product of independent probabilities:

$$E\left[\max\left(\hat{f}_m(\boldsymbol{x}^*) - \hat{f}_m(\boldsymbol{x}), 0\right) \cap \{g > g_{\min}\}\right] \;=\; E\left[\max\left(\hat{f}_m(\boldsymbol{x}^*) - \hat{f}_m(\boldsymbol{x}), 0\right)\right] \times P\left[g > g_{\min}\right] \tag{44}$$

In this fully probabilistic approach, the penalty-based objective function f in Eq. **(40)** is simply replaced by $f = C_{D,i}$, $E\left[\max\left(\hat{f}_m(\boldsymbol{x}^*)-\hat{f}_m(\boldsymbol{x}),0\right)\right]$ is calculated according to **(25)** using $s_m(\boldsymbol{x}) = s_m(C_{D,i};\boldsymbol{x})$, and

$$\begin{aligned} P\left[\hat{g}_m(\boldsymbol{x}) > g_{\min}\right] &= \int_{g_{\min}}^{+\infty} \boldsymbol{\phi}(y-\hat{g}_m(\boldsymbol{x});s_m(g;\boldsymbol{x}))\,dy \\ &= \frac{1}{2}\left[1 + erf\left(\frac{\hat{g}_m(\boldsymbol{x})-g_{\min}}{\sqrt{2}.s_m(g;\boldsymbol{x})}\right)\right] \stackrel{\text{def}}{\equiv} \boldsymbol{\psi}(\hat{g}_m(\boldsymbol{x})-g_{\min};s_m(g;\boldsymbol{x})) \end{aligned} \quad \textbf{(45)}$$

Thus, in the above example, and provided the above-mentioned independence assumptions hold, **(25)**, **(41)** and **(42)** are replaced by

$$\begin{aligned} &E\left[\max\left(\hat{f}_m(\boldsymbol{x}^*)-f_m^p(\boldsymbol{x}),0\right)\cap\left\{g > g_{\min}\right\}\right] = \\ &\quad\left[\left(\hat{C_{D,i_m}}(\boldsymbol{x}^*)-\hat{C_{D,i_m}}(\boldsymbol{x})\right).\boldsymbol{\psi}\left(\hat{C_{D,i_m}}(\boldsymbol{x}^*)-\hat{C_{D,i_m}}(\boldsymbol{x});s_m(C_{D,i};\boldsymbol{x})\right)\right. \\ &\quad\left.+\quad s_m(C_{D,i};\boldsymbol{x}).\boldsymbol{\phi}\left(\hat{C_{D,i_m}}(\boldsymbol{x}^*)-\hat{C_{D,i_m}}(\boldsymbol{x});s_m(C_{D,i};\boldsymbol{x})\right)\right] \\ &\times\left[\boldsymbol{\psi}\left(75-\left(\hat{C}_L(\boldsymbol{x})+\frac{\hat{W_{\text{wing}}}(\boldsymbol{x})}{40.76\times 5}\right)_m;\sqrt{s_m^2(C_L;\boldsymbol{x})+\frac{s_m^2(W_{\text{wing}};\boldsymbol{x})}{(40.76\times 5)^2}}\right)\right] \\ &\times\left[\boldsymbol{\psi}\left(\left(\frac{\hat{\sigma_{VM}}(\boldsymbol{x})}{\sigma_{\text{VM,max}}}\right)_m-0.5;s_m\left(\frac{\sigma_{VM}}{\sigma_{\text{VM,max}}};\boldsymbol{x}\right)\right)\right] \end{aligned} \quad \textbf{(46)}$$

which explicitly takes into account the estimated variances $s_m(C_{D,i};\boldsymbol{x})$, $s_m(C_L;\boldsymbol{x})$, $s_m(W_{\text{wing}};\boldsymbol{x})$, and $s_m(\sigma_{VM}/\sigma_{\text{VM,max}};\boldsymbol{x})$ for all the dependent variables participating in either the objective or the constraints.